



NRL/MR/7140--05-8835

Application of Differential Geometry to Acoustics: Development of a Generalized Paraxial Ray-Trace Procedure from Geodesic Deviation

DAVID R. BERGMAN
Saint Peter's College
Jersey City, NJ

January 18, 2005

Approved for public release; distribution is unlimited.

REPORT DOCUMENTATION PAGE

Form Approved
OMB No. 0704-0188

Public reporting burden for this collection of information is estimated to average 1 hour per response, including the time for reviewing instructions, searching existing data sources, gathering and maintaining the data needed, and completing and reviewing this collection of information. Send comments regarding this burden estimate or any other aspect of this collection of information, including suggestions for reducing this burden to Department of Defense, Washington Headquarters Services, Directorate for Information Operations and Reports (0704-0188), 1215 Jefferson Davis Highway, Suite 1204, Arlington, VA 22202-4302. Respondents should be aware that notwithstanding any other provision of law, no person shall be subject to any penalty for failing to comply with a collection of information if it does not display a currently valid OMB control number. **PLEASE DO NOT RETURN YOUR FORM TO THE ABOVE ADDRESS.**

1. REPORT DATE (DD-MM-YYYY) 18-01-2005			2. REPORT TYPE Memorandum		3. DATES COVERED (From - To) June 2002-August 2004	
4. TITLE AND SUBTITLE Application of Differential Geometry to Acoustics: Development of a Generalized Paraxial Ray-Trace Procedure from Geodesic Deviation					5a. CONTRACT NUMBER	
					5b. GRANT NUMBER	
					5c. PROGRAM ELEMENT NUMBER 61153N	
6. AUTHOR(S) David R. Bergman*					5d. PROJECT NUMBER	
					5e. TASK NUMBER UW032-02-43	
					5f. WORK UNIT NUMBER 71-7810	
7. PERFORMING ORGANIZATION NAME(S) AND ADDRESS(ES) Naval Research Laboratory, Code 7140 4555 Overlook Avenue, SW Washington, DC 20375-5320					8. PERFORMING ORGANIZATION REPORT NUMBER NRL/MR/7140--05-8835	
9. SPONSORING / MONITORING AGENCY NAME(S) AND ADDRESS(ES) Office of Naval Research 800 North Quincy Street Arlington, VA 22217-5660					10. SPONSOR / MONITOR'S ACRONYM(S) ONR	
					11. SPONSOR / MONITOR'S REPORT NUMBER(S)	
12. DISTRIBUTION / AVAILABILITY STATEMENT Approved for public release; distribution is unlimited.						
13. SUPPLEMENTARY NOTES *Saint Peter's College, Jersey City, NJ 07306						
14. ABSTRACT In this report, the application of abstract differential geometry to geometric acoustics is explored. The results of this application are: (1) a generalized paraxial ray-trace procedure valid for acoustic propagation in a random media with subsonic flow, (2) the demonstration of a continuum of equivalent paraxial systems related by a conformal transformation, and (3) a unified approach to treating problems in acoustics, which leads to generalized versions of Snell's law, Fermat's principle, and range- and travel-time integrals for layered media. The geodesic deviation vector is used to model beam deformation and provides one with an all-purpose tool for measuring geometric transmission loss and locating caustics within a ray skeleton without repeatedly solving the ray equations. When applied to layered media, the deviation vector is solved exactly. Compared to traditional approaches, the results are equivalent. However, the difference is vast when implemented in numerical ray-trace codes. Applications are made to several depth-dependent scenarios, including piecewise-linear sound-speed and fluid-velocity profiles for which the exact caustic structures are determined.						
15. SUBJECT TERMS Underwater acoustics; Propagation; Geodesic deviation; Ray tracing; Geometric acoustics; Subsonic flow						
16. SECURITY CLASSIFICATION OF:			17. LIMITATION OF ABSTRACT UL	18. NUMBER OF PAGES 66	19a. NAME OF RESPONSIBLE PERSON Daniel Wurmser	
a. REPORT Unclassified	b. ABSTRACT Unclassified	c. THIS PAGE Unclassified			19b. TELEPHONE NUMBER (include area code) (202) 404-4817	

CONTENTS

INTRODUCTION	1
GENERALIZED PARAXIAL RAY TRACING	3
CONFORMALLY-EQUIVALENT RAY SYSTEMS.....	14
EXAMPLES	19
DISCUSSION AND CONCLUSION.....	36
ACKNOWLEDGEMENTS.....	37
REFERENCES	37
APPENDIX A: CONCEPTS FROM DIFFERENTIAL GEOMETRY.....	40
APPENDIX B: NULL GEODESICS AND ACOUSTIC RAYS.....	45
APPENDIX C: CONSTRUCTION OF THE INTERNAL FRAME FIELD	53
APPENDIX D: RIEMANN TENSOR AND CHRISTOFFEL SYMBOLS FOR THE ACOUSTIC METRIC	57
APPENDIX E: FERMAT'S PRINCIPLE AND SNELL'S LAW.....	59

FIGURES

1. SPACE-TIME GEODESIC DEVIATION.....	5
2. EQUAL-TIME DEVIATION	5
3. BEAM DEFORMATION	6
4. INITIAL WAVEFRONT	11
5. CAUSTIC DETAIL	20
6. RAY FAN FOR CANONICAL MUNK PROFILE.....	20
7. CAUSTIC STRUCTURE FOR A HARMONIC WAVEGUIDE.....	23
8. CONVERGENCE/DIVERGENCE ZONES FOR A QUADRATIC FLUID DUCT	25
9. SAMPLE RAY FAN AND CAUSTIC DETAIL FOR A QUADRATIC FLUID DUCT.....	26
10. CONVERGENCE/DIVERGENCE ZONES FOR LINEAR SOUND-SPEED AND FLUID PROFILES	28
11. PIECEWISE-LINEAR ENVIRONMENTAL PROFILES.....	29
12. JACOBI FIELD, PIECEWISE PROFILE	30
13. RAY FAN INCIDENT ON A LINEAR HALF SPACE	34
14. SOUND-SPEED PROFILE	36
15. CAUSTIC DETAIL FOR A WEDGE DUCT	36
16. JACOBI FIELD	37
B1. SAMPLE OF A COMPLETE SPACE-TIME RAY STRUCTURE.....	51
B2. RELATIONSHIP BETWEEN FLUID VELOCITY, RAY TANGENT, AND WAVEFRONT NORMAL	51

TABLES

1. RAY-THEORY AND DIFFERENTIAL-GEOMETRY ANALOGUES.....	4
--	---

NOTATION

E^3	Euclidean space
M	Abstract manifold
x_k	Cartesian coordinates in E^3
\vec{v}	Vector in E^3
x^α	Coordinates in an open patch of M
$T_p(M)$	Tangent space at a point $p \in M$
$T_p^*(M)$	Cotangent space at a point $p \in M$
V^α	Components of an element of $T_p(M)$, contravariant vector
V_α	Components of an element of $T_p^*(M)$, covariant vector
$\Gamma^\mu_{\alpha\beta}$	Christoffel symbols of the second kind
$\{\mu; \alpha\beta\}$	Christoffel symbols of the first kind
$R_{\mu\alpha\nu\beta}$	Riemann curvature tensor
$\langle a_i \rangle$	Hyperplane spanned by the vectors $\{a_i\}$
$\langle a b \rangle$	Inner product of vectors a and b (abstract notation)
$\vec{u} \cdot \vec{v}$	Dot product of two vectors in E^3
$\vec{u} \times \vec{v}$	Cross product of two vectors in E^3
\dot{f}	Total derivative with respect to the independent parameter, df/dt , $df/d\lambda$, etc., depending on context
f'	Spatial derivative when f depends on only one space variable, df/dz
$\vec{\nabla}$	Gradient operator in E^3
(∇)	Column vector with components ∂_i
$(\nabla)^T$	Row vector, $(\partial_x \ \partial_y \ \partial_z)$
D_μ	Covariant derivative operator in M
$d_{\vec{A}}$	Total directional derivative along \vec{A} , $\partial_t + \vec{A} \cdot \vec{\nabla}$
d	Total derivative in E^3 , $\partial_t + \dot{\vec{r}} \cdot \vec{\nabla}$
$\vec{A} \otimes \vec{B}$	Direct product tensor of two vectors with components $A_j B_i$
S_{jk}	Fluid shear-compression tensor $\partial_j v_k + \partial_k v_j$
ω_{jk}	Fluid vorticity $\partial_j v_k - \partial_k v_j$

Latin indices, k , run from 1 to 3, and Greek indices, α , run from 0 to 3, with “0” reserved for the time coordinate. The Einstein summation convention is used with sum implied when any index appears only twice as a subscript in E^3 , and once as a subscript and once as a super script in M , i.e.

$$A_k B_k = \sum_{k=1}^3 A_k B_k, \quad A_\alpha B^\alpha = \sum_{\alpha=0}^3 A_\alpha B^\alpha.$$

APPLICATION OF DIFFERENTIAL GEOMETRY TO ACOUSTICS: DEVELOPMENT OF A GENERALIZED PARAXIAL RAY-TRACE PROCEDURE FROM GEODESIC DEVIATION

1. INTRODUCTION

When background fluid motion is subsonic the acoustic rays in a time-dependent moving ideal fluid are equivalent to the null geodesics of a pseudo-Riemannian manifold^{1,2}. This connection suggests a novel approach to dealing with linear acoustics. Equating the features of ray theory with concepts from differential geometry offers an advantage to traditional views by:

- Providing a unified approach to problems in acoustics that encapsulates all known results in an easily accessible format.
- Leading to immediate generalizations of known problems that include the effects of random media on the acoustic field.

Specifically, by using geometric principles this approach leads to generalized versions of Fermat's principle, ray integrals for layered moving media, Snell's law, and the laws of geometric spreading. In addition to reproducing known results, the application of differential geometry leads to a generalized version of paraxial ray tracing^{3,4} derived from the law governing geodesic deviation⁵⁻⁹. The differential geometric approach to ray tracing also offers a new way to look at different presentations of ray theory as being related by a type of geometric invariance called conformal invariance¹⁰. Conformal invariance allows one to view traditional approaches to ray theory as belonging to a continuum of equivalent representations.

Paraxial ray-trace procedures calculate ray paths within a ray bundle by solving a system of second-order linear differential equations along one ray path rather than repeatedly solving the ray equation with different initial conditions^{3,4,11}. From the results of this procedure the neighboring rays close to a specific solution of the ray equations may be mapped thus allowing one to model the deformation of a ray bundle as it propagates through a random environment. This type of ray tracing has become widely used in seismology where motion of the medium can be ignored.

The approach presented here finds its natural home in the time domain treating acoustic rays as trajectories, or histories, in space and time in contrast to the traditional view which treats the rays as unit-speed curves in space. In the conventional approach a ray trace is viewed as static structure in space, sometimes called a skeleton upon which the field flesh lives. In contrast, the space-time approach views the rays as encoding

information about the history and future evolution of the acoustic field as well as its shape at any given instant. This information is contained in the geometry of the “acoustic metric” and can be thought of as a property of the medium itself for any source placement and geometry.

Rays emerge as a high-frequency approximation to the wave theory of light or sound. The theory of bicharacteristics is more general, describing the propagation of a surface of initial data through space-time^{22,23}. The geodesic structure that determines the rays in the high-frequency limit is identical in form to that of the bicharacteristics of the field equations.

The rate of separation of neighboring geodesics from a specified geodesic with similar initial conditions is determined by the stationary values of the variation of the geodesic path with respect to initial conditions. This variation is measured by the Jacobi field of the corresponding geodesic equation determined by the second variation of the action. The same concept gives rise to the notion of geodesic deviation, a technique used in general relativity to describe gravitational tidal forces⁵⁻⁷.

Most of the applications presented in this report make use of the Jacobi field to directly calculate or estimate relevant aspects of an acoustic ray skeleton and the acoustic field. Once the Jacobi field is known for a given situation, either analytically or numerically, it can be used to calculate the:

1. Field intensity in the limit of geometric acoustics.
2. Coordinates of rays near a pre-chosen central ray within the ray skeleton.
3. Exact location of caustics along the central ray.

The behavior of the Jacobi field is determined by the Riemann curvature tensor derived from the acoustic metric—see Appendix A for details. Briefly, a positive curvature causes convergence of neighboring geodesics with a common point source and predicts the existence of conjugate points, equivalent to caustic formation in the acoustic field. Negative curvature leads to divergence of geodesics with a common point source, at roughly an exponential rate, while zero curvature leads to linear divergence. For the special case of constant curvature the manifolds described by the previous cases correspond to a sphere, pseudosphere, and Euclidean space, respectively. The relation between the environment and the Riemann curvature tensor allows one to determine, by inspection in many cases, whether or not convergence is eminent, and even estimate the frequency of caustic formation without explicitly solving for the Jacobi field. For example, stationary fluids with depth-dependent sound speeds satisfying $c''(z) > 0$, such as the canonical Munk profile used to describe the deep underwater sound channel, are known to produce natural sound ducts giving rise to nontrivial caustic structure in the acoustic field. The curvature in such cases is proportional to $c''(z)$, corresponding to locally spherical geometry. The table below provides a list of terms from ray theory and the corresponding, or relevant, differential geometric quantities. Each ray quantity is either identical to, or is derived from, the corresponding geometric quantity.

Ray Theory	Differential Geometry
Ray	Geodesic
Derivative of ray coordinates with respect to initial conditions	Jacobi field, Geodesic deviation
Rays and wavefronts for a point source	Geodesic polar mapping
Caustics	Conjugate points
Energy conservation, Fermat's principle	Null constraint
Ray integrals for layered media, Snell's law	Isometry, Symmetry of the metric tensor
Focusing effects of the medium	Riemann curvature tensor

Table 1. Ray-theory and differential-geometry analogues

The main purpose of this report is to present a complete set of paraxial ray equations for three- and four-dimensional acoustic ray tracing in an arbitrary environment, including fluid motion and time dependence¹²⁻²¹, along with illustrative examples employing the techniques of differential geometry, and to discuss the conformally-equivalent representations of ray theory.

In Section 2 the complete paraxial ray-tracing procedure is presented in four-dimensional space-time and three-dimensional space, along with detailed descriptions of the quantities involved. The special case of layered media leads to an exact solution for the Jacobi field. Section 3 describes the effects of conformal invariance in stationary fluid systems and compares the results for four different popular choices of ray parameter. Section 4 presents an analysis of several systems that have exact solutions for the rays and the Jacobi field, and describes the caustic structure as predicted by the Jacobi field. Appendix A provides a list of relevant concepts from differential geometry as a quick reference for the reader. The reader interested in a deeper presentation should consult Refs. 7, 8, and 24. Appendix B presents a complete derivation of the geodesic structure associated with the bicharacteristics beginning from first principles, comparing the general case to that of linear acoustics in the high-frequency limit. Appendix C presents the technical details behind constructing a ray-centered basis for the paraxial ray-trace procedure. Appendix D lists the components of the Christoffel symbols of the second kind and the Riemann curvature tensor in a Cartesian coordinate basis, while Appendix E introduces isometry and derives the ray integrals along with Snell's law for layered media with linear and polar symmetries. While Appendices A, B, and E are mostly for completeness and rigor, Appendices C and D are an integral part of the paraxial ray-trace procedure.

2. GENERALIZED PARAXIAL RAY TRACING

In this section the complete generalized paraxial ray-tracing procedure is presented in affine and time parameterizations along with results for layered media. Figure 1 illustrates the basic features of a ray system in a two-dimensional slice of space-time. The fiducial ray is labeled γ_F and neighboring rays are labeled γ_N . The coordinates of

each ray are x_F^μ and x_N^μ respectively, and are related by $x_N^\mu = x_F^\mu + Y^\mu$. The choice of ray parameter used in the geometric approach corresponds to an affine parameter, labeled λ . The significance of λ is discussed in Appendix A.4. The ray tangent, T^μ , in space-time and the deviation vector, Y^μ , at two values of the affine parameter, λ , are shown. The deviation vector lies in a 2-dimensional space-like hyperplane at each point of the ray γ_F . The Jacobi equation describes the evolution of this vector projected into this hyperplane and requires the introduction of a ray-centered orthonormal basis $\langle \hat{e}_I \rangle$, $I = 1, 2$ (not shown in the figure). In general, the deviation vector will turn into the time direction while always remaining space-like.

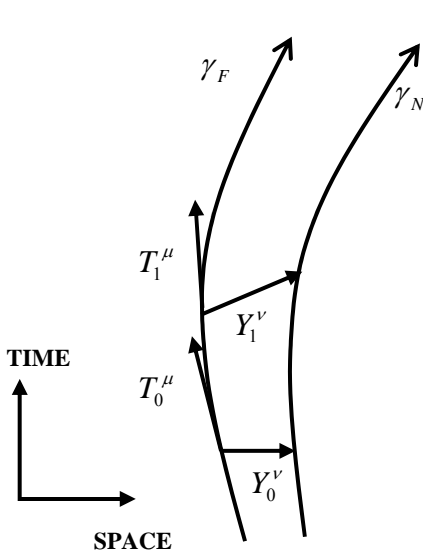


Figure 1. A fiducial geodesic and one of its neighbors are shown, along with the fiducial tangent vector and the 4-D deviation vector at two values of λ , labeled 0 and 1.

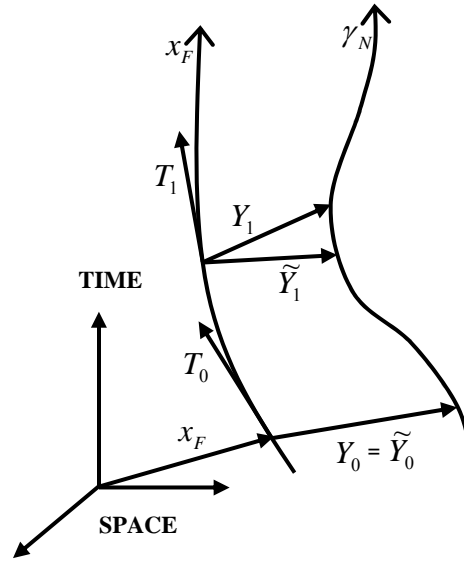


Figure 2. Similar to Fig. 1 but including the equal-time deviation vector, shown at both points along the fiducial ray. The 4-D and 3-D deviation vectors are initially equal by choice. As the system is tracked along γ_F , Y picks up a time-like component while \tilde{Y} contains only space-like components at all times.

Coordinate time is a more natural choice of ray parameterization from the physical point of view. In the coordinate-time-parameterized version of the problem, the deviation vector remains tangent to the wavefront in space at all points along the ray—see Fig. 2. In this case, the deviation vector approximates a small arc in the eikonal surface and may be used to reconstruct the wavefront in a small region about the central ray by sweeping the deviation vector about the central ray for a complete set of initial launch angles, forming a small disk (Fig. 3).

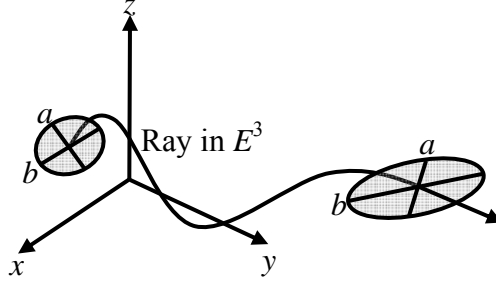


Figure 3. A 3-D ray path is shown along with a small ring formed by the locus of initial 3-D deviation vectors. As the deviation vectors are propagated along the ray this ring deforms as a result of the local refractive index and fluid velocity. A pair of axes, labeled a and b , are included to demonstrate the change of orientation of the wavefront.

2.1 Affine Representation

The paraxial equations consist of three main ingredients: the geodesic equation, the parallel transport equation, and the Jacobi equation, respectively listed below:

$$\frac{d^2 x^\mu}{d\lambda^2} + \Gamma^\mu_{\alpha\beta} \frac{dx^\alpha}{d\lambda} \frac{dx^\beta}{d\lambda} = 0, \quad (1)$$

$$\frac{de_i^\mu}{d\lambda} + \Gamma^\mu_{\alpha\beta} \frac{dx^\alpha}{d\lambda} e_i^\beta = 0, \quad (2)$$

$$\frac{d^2 Y_I}{d\lambda^2} + K_{IJ} Y_J = 0, \quad (3)$$

where

$$Y_I = \hat{e}_I^\alpha g_{\alpha\beta} Y^\beta, \quad (4)$$

$$K_{IJ} \equiv R_{\mu\alpha\nu\beta} \dot{x}^\alpha \dot{x}^\beta \hat{e}_I^\mu \hat{e}_J^\nu. \quad (5)$$

The explicit forms of $\Gamma^\mu_{\alpha\beta}$ and $R_{\mu\alpha\nu\beta}$ appear in Appendix D. Many of the longer equations will be found in Appendices B–D along with derivations.

The paraxial ray-tracking procedure may be outlined as follows:

1. Find a specific solution to the geodesic equation, Eq. (1), labeled the fiducial geodesic, $\gamma_F(\lambda)$.
2. Solve the parallel transport equation, Eq. (2), for the ray-centered basis \hat{e}_I^α along $\gamma_F(\lambda)$.
3. Using the results of steps 1 and 2 solve the Jacobi equation, Eq. (3), for some specified initial conditions $\{\alpha\}$ to get the components of the deviation vector Y_I along $\gamma_F(\lambda)$ projected onto the internal basis.
4. The space-time components of the deviation vector, $Y^\mu = Y_I \hat{e}_I^\mu$, give the coordinates of a neighboring ray, $x_N^\mu = x_F^\mu + Y^\mu$.

Expanding upon the above procedure provides the necessary information for calculating the geometric spread of the acoustic beam in space-time.

5. Repeat step 3 by either:
 - a. Choosing a new set of initial conditions $\{\tilde{\alpha}\}$ on Y_I , such that $Y_I(\alpha, \lambda) \cdot Y_I(\tilde{\alpha}, \lambda) = 0$.
 - b. Rotating the initial deviation $Y(\alpha)$ in the $\langle \hat{e}_I \rangle$ plane by a small change of initial conditions.
6. The infinitesimal cross-sectional area of the ray bundle in the $\langle \hat{e}_I \rangle$ plane is then respectively given by:
 - a. $Y(\alpha) \times Y(\tilde{\alpha})$.
 - b. $Y(\alpha) \times dY(\alpha)/2$.

The order of the geodesic and deviation equations is reduced by introducing new variables $p^\alpha = \dot{x}^\alpha$ and $P_I = \dot{Y}_I$ and defining a 20-dimensional dynamic vector,

$$u = x^\alpha \oplus p^\alpha \oplus e_I^\alpha \oplus Y_I \oplus P_I \quad , \quad I = 1, 2. \quad (6)$$

The complete paraxial equations are then

$$\frac{du}{d\lambda} = F(u, \dot{u}) \quad (7)$$

with

$$F(u, \dot{u}) = p^\alpha \oplus -\Gamma^\alpha_{\mu\nu} p^\mu p^\nu \oplus -\Gamma^\alpha_{\mu\nu} p^\mu e_I^\nu \oplus P_I \oplus -K_{IJ} Y_J. \quad (8)$$

The 20 equations are subject to 8 constraints. Provided the initial data satisfy these constraints, the solution will always satisfy them in principle. There are 7 constraints on the 8 components of e_I^α (see Appendix C) and one constraint on p^α . Implementing all of the constraints reduces the dynamical system to 12 degrees of freedom:

$$u = x^k \oplus p^k \oplus t \oplus R(\alpha) \oplus Y_I \oplus P_I, \quad (9)$$

where t is coordinate time. The corresponding derivative vector is of the form

$$F(u, \dot{u}) = p^k \oplus A^k \oplus w \oplus \tilde{\omega} \oplus P_I \oplus -K_{IJ} Y_J, \quad (10)$$

where $w \equiv dt/d\lambda$ is determined by the null constraint, Appendix B.4, Eq. (B.15), $A^k = -\Gamma^k_{\alpha\beta} p^\alpha p^\beta$, with all occurrences of p^0 replaced using the null constraint and that $R(\alpha)$ is an SO(2) rotation. Imposing the constraints on the system does not necessarily lead to a simpler system. The reduction of variables leads to an increased complexity in the remaining equations, and the quantities $\tilde{\omega}$ and w typically contain denominators that may vanish on occasion.

An important consequence of this construction is that the deviation vector points in four-dimensional space-time from the fiducial geodesic, $\gamma_F(\lambda)$, to a point on a neighboring geodesic, $\gamma_N(\lambda)$, with the same value of affine parameter λ . This means that the deviation vector will not necessarily remain “in phase” with the fiducial ray path in the traditional sense of the term. This does not pose any problems in the geometric description of neighboring curves since the Jacobi field simply maps out the local space-time geometry in a tube surrounding $\gamma_F(\lambda)$ without prejudice to any coordinate, time being just another coordinate in the four-dimensional geometric paradigm. Two adjustments can be made which render the system of Eqs. (1)–(5) useful for reconstructing the wavefronts and predicting geometric loss. These two adjustments are independent of each other and the resulting procedure is identical to that outlined above.

2.2 Time Parameterization

Including the auxiliary basis described in Appendix C to the above procedure allows for the identification of neighboring points on the wavefront at a given value of λ by using the data for p^μ and \hat{e}_I^μ to construct \tilde{e}_I (see Appendix C.2, Eq. (C.3), for an explicit form of \tilde{e}_I). Switching to a coordinate-time parameterization of the problem allows \tilde{e}_I to be tracked directly without the need for \hat{e}_I^0 , eliminates the need for calculating time, and allows one to easily construct wavefronts from ray data by

specifying that the ray equations be integrated to a given set of time values. The corresponding equations and dynamical vector are listed below:

$$\begin{aligned} \ddot{x}_k = & \frac{(\dot{x}_k - v_k)}{2c^2} S_{ij} (\dot{x}_i - v_i) (\dot{x}_j - v_j) + (\dot{x}_k - v_k) (d_{-\bar{v}} \ln c + 2\dot{r} \cdot \bar{\nabla} \ln c) \\ & + \partial_t v_k - c \partial_k c - \omega_{kj} (\dot{x}_j - v_j) + \frac{1}{2} (S_{kj} - \omega_{kj}) v_j, \end{aligned} \quad (11)$$

$$\frac{d}{dt} \tilde{e}_{I,k} + \frac{1}{2} \varepsilon_{jki} (\bar{\nabla} \times \bar{v} + \bar{s} \times \hat{n} + 2\bar{\nabla} c \times \hat{n})_j \tilde{e}_{I,i} = 0, \quad (12)$$

$$\frac{d^2 Y_J}{dt^2} - \kappa \frac{dY_J}{dt} + \tilde{K}_{IJ} Y_I = 0, \quad (13)$$

with $\kappa \equiv \Gamma^0_{mn} t^m t^n + \Gamma^0_{00} + 2\Gamma^0_{m0} t^m$ and $\tilde{K}_{IJ} = (R_{\mu 0 \nu 0} + R_{\mu m \nu n} t^m t^n + 2R_{\mu 0 \nu n} t^n) \hat{e}_I^\mu \hat{e}_J^\nu$.

Derivations of each formula are given in the appendices. The time-parameterized representation of the equations requires a 16-dimensional dynamical array

$$u = \bar{x} \oplus \bar{p} \oplus \tilde{e}_I \oplus Y_I \oplus P_I, \quad (14)$$

with derivative vector given by

$$F = \bar{p} \oplus \bar{A} \oplus \Omega \tilde{e}_I \oplus P_I \oplus -\tilde{K}_{IJ} Y_J. \quad (15)$$

Imposing constraints in the auxiliary basis leads to an 11-dimensional system. This is not a huge improvement to the 12-dimensional array of the last section. However there are a few attractive features of this representation of the problem. First, there is no equation for determining travel time along the ray path since time is the parameter used as a step in the integration of the system. Second, the equations are free of any divisions that might go to zero during the procedure. Finally, there is the conceptual or pedagogical advantage of being able to immediately identify the wavefronts from the data without any additional work. The equations do involve a greater number of terms as compared to the affine counterpart, introducing greater complexity. The vector \tilde{Y}_I measures the deviation within the wavefront.

2.3 Two Spatial Dimensions

Many systems of interest in acoustic modeling are either legitimately two-dimensional or can be reduced to effective two-dimensional systems that provide good approximations to the true system. In such cases the auxiliary basis vector is completely determined at all points along the ray by a 90-degree rotation of the wavefront normal. The reduction of spatial dimensions also reduces the number of components of the

deviation vector from 2 to 1. In the affine parameterization there are 8 degrees of freedom:

$$u = x^\alpha \oplus p^\alpha \oplus Y \oplus P. \quad (16)$$

Moving to a time parameterization further reduces the system to 6 dimensions:

$$u = \bar{x} \oplus \bar{p} \oplus Y \oplus P. \quad (17)$$

Not only is the work required to produce the answer significantly reduced, but also the equations are usually simpler in form for lower-dimensional systems. The basic steps in the procedure are identical to those outlined for the affine case.

2.4 Initial Conditions, Mapping of Neighboring Rays, and Beam Deformation

The components of the equal-time deviation vector \tilde{Y}_l approximate a small element of arc length within the eikonal surface in the \tilde{e}_l direction. The initial value of the deviation may be chosen arbitrarily. The initial value of \dot{Y}_l may also be chosen arbitrarily and is related to the values of the physical parameters that describe the environment. In modeling the evolution of a wavefront the initial geometry is assumed known, hence it is desirable to express \dot{Y}_{l0} in terms of known quantities. By definition $x_N^\mu = x_F^\mu + Y^\mu$, $\dot{Y}^\mu = \dot{x}_N^\mu - \dot{x}_F^\mu$, and $d\bar{x}_F/d\lambda = dt_F/d\lambda(c_F\hat{n}_F + \bar{v}_F)$, with a similar expression for the neighboring ray, $c_F \equiv c(x_F^\mu)$ being a shorthand notation for the local sound speed evaluated at a point on the fiduciary ray (with similar expressions for all other quantities evaluated along the ray). At the initial wavefront $t_F|_0 = t_N|_0$ by choice, and the initial rates may be chosen such that $dt_F/d\lambda|_0 = dt_N/d\lambda|_0$. Denoting this common initial rate of the time coordinate by the constant β , the initial velocity of the deviation vector becomes $\dot{Y}_0 = \beta(c_N\hat{n}_N - c_F\hat{n}_F + \bar{v}_N - \bar{v}_F)$, all quantities being evaluated at the same λ but along different rays. In terms of time parameterization $d\bar{Y}/dt|_0 = c_N\hat{n}_N - c_F\hat{n}_F + \bar{v}_N - \bar{v}_F$, and the initial deviation velocity for two rays with a common initial position $d\bar{Y}/dt|_0 = c_0\Delta\hat{n}$, where $\Delta\hat{n} \equiv \hat{n}_N - \hat{n}_F$ with both terms being evaluated at the same point in space. The quantity $\Delta\hat{n}$ determines the initial shape of the wavefront, whereas all other quantities are assumed to be given (see Fig. 4).

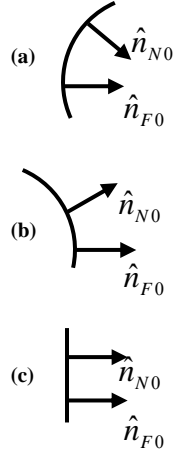


Figure 4. The shape of a small patch of the initial wavefront and two neighboring wavefront normal vectors are depicted for the three cases, a: (a) concave, (b) convex, and (c) planar section of the wavefront.

The initial values of \dot{Y}_I may be expressed in terms of \dot{Y}_0^μ . By explicitly differentiating the expression $Y_I = Y^\mu \hat{e}_{I\mu}$, the following expressions for the initial values of \dot{Y}_I are derived:

$$\left. \frac{dY_I}{d\lambda} \right|_0 = \beta \hat{e}_I^k \Big|_0 \left\{ \left. \frac{dY^k}{d\lambda} + \frac{1}{2} Y^i \omega_{ki} \right\} \Big|_0, \quad (18)$$

where all values are taken at the initial point along $\gamma_F(\lambda)$, and $dY^k/d\lambda|_0$ is given in the previous paragraph in terms of data at the initial point, along both $\gamma_F(\lambda)$ and $\gamma_N(\lambda)$. Dividing by β in Eq. (18) gives the appropriate initial values for dY_I/dt . Given a specific choice of initial wavefront geometry at a specific position in space-time, Eq. (18) gives the appropriate initial conditions for $dY_I/d\lambda$ or dY_I/dt .

Intuitively caustics, or focal points, along a ray may be identified with points where $Y^\mu = 0$. To be more explicit the deviation vector is expressed as a function of the initial conditions $Y(\lambda; (Y_0, \dot{Y}_0)) \equiv Y_\lambda(a_i)$, where $(Y_0, \dot{Y}_0) \equiv a_i$ is a shorthand notation referring to the set of initial conditions along the i -th neighboring ray to $\gamma_F(\lambda)$ (with coordinate indices suppressed). If the initial conditions of the family of neighboring rays are close to those of the fiduciary ray (which is necessarily true), then a caustic point along $\gamma_F(\lambda)$ is determined by $Y_\lambda(a_i) = 0$. It may happen that two different neighboring rays, say $\gamma_{N_1}(\lambda)$ and $\gamma_{N_2}(\lambda)$, with similar initial conditions meet without ever encountering

$\gamma_F(\lambda)$. If the two sets of initial conditions are close to each other a crossing of this pair is determined by the condition $Y_\lambda(a_1) = Y_\lambda(a_2)$.

By applying step 6b a picture of the beam cross section at any later time may be constructed. The area of the planar cross section is calculated from

$$A(t) = \frac{1}{2} \left| \oint \tilde{Y}(t) \times d\tilde{Y}(t) \right|, \quad (19)$$

where \tilde{Y} and $d\tilde{Y}$ may be expressed in terms of a_i and da_i . The acoustic intensity at any point along the ray is determined from the cross-sectional area of the ray bundle. From the differential area element $dA\hat{n}$ determined in step 5, one obtains

$$I_0/I_t = (dA\hat{n} \cdot \hat{t})_t / (dA\hat{n} \cdot \hat{t})_0, \quad (20)$$

where \hat{t} is a unit vector tangent to the ray path and \tilde{Y} is projected in the wavefront normal basis.

2.5 Application to Layered Media

To find an explicit expression for the deviation vector the tangent of the fiduciary ray and the basis vectors along the ray must be known at every point. For two-dimensional problems involving layered media it is always possible to find closed-form expressions for these quantities. To achieve this the explicit form of the geodesic equation, Eq. (1), is abandoned in favor of a set of first-order equations derived from identifying isometries of the metric tensor (Appendix E).

Consider a medium with sound speed $c(z)$ and one-dimensional fluid velocity of the form $v_x(z) \equiv v(z)$. Rays, considered as curves in E^3 , that are initially fired in the x - z plane do not turn out of their initial osculating plane, i.e. are torsion free, and constitute an effective two-dimensional system. The components of the ray velocity follow immediately from the procedure in Appendix E:

$$\frac{dt}{d\lambda} = \frac{\kappa_0}{c^2} (1 - v\alpha) \quad , \quad (21)$$

$$\frac{dx}{d\lambda} = \kappa_0 \alpha + \kappa_0 \frac{v}{c^2} (1 - v\alpha) \quad , \quad (22)$$

$$\frac{dz}{d\lambda} = \pm \frac{\kappa_0}{c} \sqrt{(1 - v\alpha)^2 - \alpha^2 c^2} \quad . \quad (23)$$

Differentiating Eq. (21) implies $c^2 \ddot{t} = -(\kappa_1 v' + 2cc't)\dot{z}$, while differentiation of Eq. (23) and use of the last result implies $\ddot{z} = -(\kappa_1 v' + cc't)\dot{t}$, where dot denotes differentiation with respect to λ . It may be demonstrated that turning points in time are not allowed, as the relation $dt/d\lambda = 0$ leads to the unphysical result $(dz/d\lambda)^2 < 0$, hence without loss of generality, the condition $dt/d\lambda > 0$ may be placed on any ray in the system.

The single basis vector for the eikonal, \tilde{e} , is constructed by simply rotating the normal $\hat{n} = d\bar{r}/dt - \bar{v}$ by $\pm 90^\circ$ in the x - z plane, giving the following expressions for the components of the second-rank antisymmetric tensor $\Lambda^{\mu\nu}$, $\hat{e}^x \dot{t} - \hat{e}^0 \dot{x} = \pm \dot{z}/c$ and $\hat{e}^z \dot{t} - \hat{e}^0 \dot{z} = \mp \kappa_1/c$, and the useful relation $\hat{e}^x \dot{z} - \hat{e}^z \dot{x} = \pm \kappa_0/c$, which is derived from the identity $T^i \hat{e}_i^k - T^k \hat{e}_i^i = T^i \tilde{e}_i^k - T^k \tilde{e}_i^i$. Thus the explicit form of the Christoffel symbols is unnecessary for determining the ray tangent and its basis.

The Cartesian components of the covariant Riemann tensor derived from the acoustic metric are listed below:

$$R_{0x0x} = -c^2 R_{xxzz} = \frac{(v')^2}{4}, \quad (24a)$$

$$R_{0xxz} = \frac{1}{4c^2} (2c^2 v'' + v(v')^2 - 2cc'v'), \quad (24b)$$

$$R_{0z0z} = -\frac{1}{4c^2} (-4c^3 c'' + 3c^2 (v')^2 + 4c^2 v v'' - 4cc'v v' + v^2 (v')^2). \quad (24c)$$

The sectional curvature along the ray derived from the Riemann tensor is

$$K = \frac{\alpha}{c^2} v'' (1 - \alpha v) - \frac{\alpha^2}{c^2} (v')^2 - \frac{\alpha}{c^3} c' v' (1 - \alpha v) + \frac{\alpha^2}{c} c'', \quad (25)$$

which may be reduced to

$$K = \frac{\kappa_0^2}{2} \frac{1}{c} \frac{d}{dz} \left(\frac{1}{c} \frac{d}{dz} (\alpha^2 c^2 - (1 - \alpha v)^2) \right).$$

The Jacobi equation then becomes

$$\frac{d^2 Y}{d\lambda^2} + KY = 0. \quad (26)$$

The last term in Eq. (25) states that c'' governs the focusing properties of a stationary medium with an inhomogeneous sound speed. A ray propagating in a region with $c'' > 0$

will eventually encounter conjugate points, while rays propagating in regions where $c'' < 0$ will diverge from one another. When the sound speed is constant the effects of fluid motion can be broken up into two terms, $\alpha v'' - (v')^2 (\alpha/c)^2$. The second term is always negative, causing ray divergence. In the first term the focusing effects are determined by the relative sign of α and v'' . This term will cause focusing of acoustic rays when α and v'' have the same sign. As a consequence a constant fluid velocity has no effect on the stability of neighboring rays, while a fluid velocity with a constant gradient will interfere with the focusing caused by an inhomogeneous sound speed with $c'' > 0$.

A more interesting situation occurs when both c and v depend on depth. The remarks of the last paragraph are still valid with the addition of an extra term coupling the sound-speed gradient to the fluid-velocity gradient, $-v'c'\kappa_1 i/c$, appearing in Eq. (25). This term is more difficult to interpret than the others contributing the curvature. Consider a simple situation in which a waveguide is created by a sound-speed profile with $c'' > 0$ everywhere. Above the waveguide axis $c' > 0$, while below the waveguide axis $c' < 0$. If the fluid motion is to the right and characterized by a uniform gradient, then $v' > 0$. For acoustic rays fired to the right $\alpha > 0$, resulting in a separation of neighboring rays above the waveguide axis and an enhanced convergence of rays below the waveguide axis. When the background fluid motion is weak and slowly varying, the leading-order terms in Eq. (25) are $\alpha v''/c^2 + \alpha^2 c''/c$, indicating that the dominant effects are due to the concavity of the environmental parameter values.

Between vertical turning points the deviation equation may be converted into a differential equation in the variable z that in general reduces to a single integral in z . Changing variables to $d\sigma = cdz$ leads to the following general solution for the Jacobi field

$$Y = \dot{z}c \left\{ c_1 \int \frac{cdz}{\dot{z}^3 c^3} + c_2 \right\}, \quad (27)$$

with constants c_1 and c_2 set to match the initial conditions of the deviation vector. For cases when $\dot{z} = 0$ identically along the ray, one cannot perform the change of variables from λ to z and such cases must be treated separately. Equation (27) can be integrated in some cases to yield a closed-form solution in terms of ordinary functions. For the case of layered stationary media Eq. (27) becomes

$$Y = \sqrt{1 - \alpha^2 c^2} \left\{ c_1 \int \frac{cdz}{(1 - \alpha^2 c^2)^{3/2}} + c_2 \right\}, \quad (28)$$

which appears in a slightly different form in Cerveny³.

3. CONFORMALLY-EQUIVALENT RAY SYSTEMS

Although this technique can be applied in general, we now apply it to two-dimensional underwater systems with range, depth and time dependence for concreteness and simplicity. The acoustic line element for stationary media in four-dimensional space-time coordinates is $-c(\bar{x}, t)^2 dt^2 + d\bar{x} \cdot d\bar{x} = 0$. In general, rays in space will not be confined to a two-dimensional plane but spiral through the medium as determined by the gradients of the sound speed. For situations in underwater acoustics one can find either effective two-dimensional subsystems within the ray structure, or in many situations the torsion of the rays is negligible for the range of interest leading to $-c(z, r, t)^2 dt^2 + dz^2 + dr^2 = 0$, with corresponding metric tensor $g_{\mu\nu} \equiv -c(z, r, t)^2 \oplus \delta_{ij}$.

As a result of conformal invariance we are free to pick and choose from a continuum of theoretically equivalent representations of the same system. Why choose a particular one over another? Common to many laws of physics is the fact that the law itself is coordinate or gauge invariant yet a specific representation must be chosen to get the problem solved. Choosing a particular representation wisely results in a simpler problem from both the analytical and numerical points of view.

Below are presented four popular choices of parameterization of the ray equations along with a comment of its use in the literature. Each is presented here as an affine parameter leading to a new geometry. In other references this is taken to be simply a change in parameter devoid of any geometric significance.

3.1 Affine Parameterization

This is the obvious choice from a geometric point of view. It appeared once in an article by R.W. White¹⁹, introducing the connection between null geodesics and acoustics rays. It also appears to be identical to the parameterization used by Cerveny in seismic ray theory³. The ray equations are:

$$\frac{d^2 t}{d\lambda^2} + \frac{1}{c} \frac{dt}{d\lambda} \left\{ \frac{dt}{d\lambda} \frac{\partial c}{\partial t} + 2 \left(\frac{dx}{d\lambda} \frac{\partial c}{\partial x} + \frac{dz}{d\lambda} \frac{\partial c}{\partial z} \right) \right\} = 0, \quad (29)$$

$$\frac{d^2 z}{d\lambda^2} + c \frac{\partial c}{\partial z} \left(\frac{dt}{d\lambda} \right)^2 = 0, \quad \frac{d^2 x}{d\lambda^2} + c \frac{\partial c}{\partial x} \left(\frac{dt}{d\lambda} \right)^2 = 0. \quad (30), (31)$$

The null condition may be used to eliminate $dt/d\lambda$ from the equations for the spatial variables if desired. Also, note that the second-order equation for time may be derived by differentiating the null constraint. When the sound speed is explicitly time dependent one cannot perform the single integration of $dt = ds/c$ unless the sound speed is a separable function, $c(t)c(\bar{r})$. The Jacobi equation for this geometry is given below in Cartesian coordinates:

$$\frac{d^2 Y}{d\lambda^2} + \frac{1}{c} \left\{ \left(\frac{dz}{d\lambda} \right)^2 \frac{\partial^2 c}{\partial x^2} + \left(\frac{dx}{d\lambda} \right)^2 \frac{\partial^2 c}{\partial z^2} - 2 \frac{dz}{d\lambda} \frac{dx}{d\lambda} \frac{\partial^2 c}{\partial x \partial z} \right\} Y = 0 \quad . \quad (32)$$

The space-time components of the ray tangent are $T^\mu = (c^{-2} \quad c^{-1} \hat{n})$, which may look a little strange at first. This is due to the nature of, and units of, the affine parameter. One can check by hand that $\langle T|T \rangle = 0$ as expected. The ray velocity in E^3 is given by $\bar{T}/T^0 = \hat{n}$ as expected. In ray-centered coordinates the Jacobi equation becomes

$$\frac{d^2 Y}{d\lambda^2} + \frac{1}{c^3} \frac{\partial^2 c}{\partial y^2} Y = 0 \quad . \quad (33)$$

Conceptually this is very easy to interpret. The stability of a ray is governed by the concavity of the sound speed in the vicinity of the ray. In practice this can be difficult to implement as we typically do not know a priori $c(y)$ (sound-speed data are usually given as $c(x,z)$). A virtue of this parameterization is the simplicity of the equations. The medium was not assumed to be time independent, yet no time derivatives of the sound speed appear in the equations for either the space coordinates of the ray or the geometric spreading.

3.2 Time Parameterization

This most closely resembles the equations found in Landau and Lifshitz²⁵. When the sound speed depends on only depth and range, the time integral can be performed along the ray path indicating that the differential equation is superfluous. Time symmetry leads to the constraint

$$c^2 \frac{dt}{d\lambda} = k_0 \quad .$$

This also indicates that travel time is a good choice of affine parameter. By simply rearranging terms in the line element we can find a representation of the geometry that allows time to be used as an affine parameter. Let $d\lambda \rightarrow d\lambda/c^2 = dt$ with $k_0 = 1$. The new space-time metric structure is $-dt^2 + (dx^2 + dz^2)/c^2 = 0$. The null surface is equivalent to a two-dimensional Riemannian surface with a line element defined by $dt^2 = (dx^2 + dz^2)/c^2$. One can think of this as a travel-time space and the proper arc length between two points is a measure of the travel time along the curve connecting them. In this representation there is no equation for time. The equations for the ray coordinates are

$$\frac{d^2 x}{dt^2} = \frac{2}{c} \frac{dx}{dt} \left(\frac{dx}{dt} \frac{\partial c}{\partial x} + \frac{dz}{dt} \frac{\partial c}{\partial z} \right) - c \frac{\partial c}{\partial x} \quad , \quad (34)$$

$$\frac{d^2 z}{dt^2} = \frac{2}{c} \frac{dz}{dt} \left(\frac{dx}{dt} \frac{\partial c}{\partial x} + \frac{dz}{dt} \frac{\partial c}{\partial z} \right) - c \frac{\partial c}{\partial z}. \quad (35)$$

The ray tangent in space-time is $T^\mu = (1 \quad c\hat{n})$ with $d\bar{r}/dt \equiv c\hat{n}$. The ray velocity has unit length with respect to the acoustic metric. The Jacobi equation for this geometry has a particularly simple form

$$\frac{d^2 Y}{dt^2} + \{c\nabla^2 c - \bar{\nabla}c \cdot \bar{\nabla}c\}Y = 0. \quad (36)$$

Some attractive features of this representation are that the sectional curvature does not depend on the ray momentum and time is used as a parameter. Ray code based on this theory does not require travel-time calculations and wavefronts can be more easily identified from numerical data. The ray equations are not terribly complicated as compared with the previous case, but the spreading equation is simpler in that it does not depend on any of the ray-momentum variables. The second term in Eq. (36) does lead to theoretically interesting changes and potential numerical effects. The curvature is a defining property of geometry. As a simple example consider the c -linear sound-speed profile as a function of depth. In the affine parameterization, this is a space of zero curvature, i.e. flat as a plane. In the time parameterization, it is a space of constant negative curvature—see Section 4 for details. Additionally, sound speeds with positive concavity can have regions of negative curvature according to Eq. (36). In cases where the ray bundles of interest are required to be parabolic this does not pose any problems. In general, it could lead to divergent behavior of Y .

3.3 Range-Independent Sound Speed

This choice of parameter is used by researchers studying ray chaos in range-dependent systems where the ray equations are viewed as a two-dimensional non-autonomous Hamiltonian system^{26,27}. It is important to note that in those cases a conformal transformation will not make r an affine parameter. This type of system has also been studied in the context of instability due to time-dependent fluctuations where this identification is possible.

The same trick used in the last section may be employed when the sound speed is of the form $c(z,t)$. In this case, beginning from the general case we have one conserved quantity, $dx/d\lambda = k_1$. This indicates that range is already an affine parameter. Rearranging the null-line element gives an effective two-dimensional Lorentzian geometry, $-dx^2 = -c^2 dt^2 + dz^2$. In this representation of the ray structure, range is the proper arc length of the acoustic line element. Notice that the line element is negative indicating that the acoustics rays in (t, z) space are identical in structure to geodesic paths corresponding to massive particle trajectories.

The ray equations are

$$\frac{d^2 t}{dx^2} + \frac{1}{c} \frac{\partial c}{\partial t} \left(\frac{dt}{dx} \right)^2 + \frac{2}{c} \frac{\partial c}{\partial z} \frac{dt}{dx} \frac{dz}{dx} = 0, \quad (37)$$

$$\frac{d^2 z}{dx^2} + c \frac{\partial c}{\partial z} \left(\frac{dt}{dx} \right)^2 = 0. \quad (38)$$

The corresponding Jacobi equation is

$$\frac{d^2 Y}{dx^2} + \frac{1}{c} \frac{\partial^2 c}{\partial z^2} Y = 0. \quad (39)$$

In this case the curvature term is independent of the ray momentum. This follows from the reduction of the problem to an effectively lower-dimensional system, and the fact that two-dimensional manifolds only have one independent component of the Riemann curvature tensor. The equations take their simplest form in this representation.

3.4 Three-Dimensional Arc Length Parameterization

This is by far the most common presentation of the ray equations found in texts on acoustics. It is used in the theoretical treatment of ray geometry in E^3 as a unit-speed curve and is the basis for a number of early ray trace codes²⁸⁻³⁰.

In general, the space-time line element implies the relation $cdt = dS$, where S is defined as three-dimensional arc length of the ray. This relation also immediately hints at an appropriate conformal transformation leading to a geometric representation in which S is an affine parameter. The general form of the complete set of equations is:

$$\frac{dt}{dS} = \frac{1}{c}, \quad (40)$$

$$\frac{d^2 x}{dS^2} = \frac{1}{c} \frac{dx}{dS} \left(\frac{\partial c}{\partial z} \frac{dz}{dS} + \frac{\partial c}{\partial x} \frac{dx}{dS} + \frac{1}{c} \frac{\partial c}{\partial t} \right) - \frac{1}{c} \frac{\partial c}{\partial x}, \quad (41)$$

$$\frac{d^2 z}{dS^2} = \frac{1}{c} \frac{dz}{dS} \left(\frac{\partial c}{\partial z} \frac{dz}{dS} + \frac{\partial c}{\partial x} \frac{dx}{dS} + \frac{1}{c} \frac{\partial c}{\partial t} \right) - \frac{1}{c} \frac{\partial c}{\partial z}, \quad (42)$$

$$\frac{d^2 Y}{dS^2} + KY = 0, \quad (43)$$

with

$$\begin{aligned}
K = & \frac{1}{2c} \frac{\partial^2 c}{\partial x^2} \left(1 + \left(\frac{dz}{dS} \right)^2 \right) + \frac{1}{2c} \frac{\partial^2 c}{\partial z^2} \left(1 + \left(\frac{dx}{dS} \right)^2 \right) - \frac{1}{2c^2} \left(\frac{\partial c}{\partial x} \right)^2 \left(1 + \frac{1}{2} \left(\frac{dz}{dS} \right)^2 \right) \\
& - \frac{1}{2c^2} \left(\frac{\partial c}{\partial z} \right)^2 \left(1 + \frac{1}{2} \left(\frac{dx}{dS} \right)^2 \right) - \frac{1}{c} \frac{dx}{dS} \frac{dz}{dS} \left(\frac{\partial^2 c}{\partial x \partial z} + \frac{1}{2c} \frac{\partial c}{\partial x} \frac{\partial c}{\partial z} \right) + \frac{1}{2c^4} \left(c \frac{\partial^2 c}{\partial t^2} - 2 \left(\frac{\partial c}{\partial t} \right)^2 \right) \\
& + \frac{1}{2c^3} \left(2c \left(\frac{dz}{dS} \frac{\partial^2 c}{\partial t \partial z} + \frac{dx}{dS} \frac{\partial^2 c}{\partial t \partial x} \right) - 3 \frac{\partial c}{\partial t} \left(\frac{dz}{dS} \frac{\partial c}{\partial z} + \frac{dx}{dS} \frac{\partial c}{\partial x} \right) \right). \tag{44}
\end{aligned}$$

One can plainly see how complicated things get in general. A significant feature of the affine parameterized equations, and the $1 \oplus 1$ -dimensional range-parameterized equations, is that the curvature tensor only depends on time through c and not its derivatives. In contrast the arc-length-parameterized representation is quite a bit more complex, even for simple systems. Virtues of this representation are that the ray momentum is $(\cos \theta \quad \sin \theta)$ and the arc length is known each step of the way.

Sample ray traces using all four approaches are given in Figs. 5 and 6, two examples each for the canonical Munk profile and the c -quadratic profile. A glance at the detail of a focal point in the c -quadratic case, Fig. 5, illustrates the precision with which each method located caustics. The different polygonal shapes due to different step-size choices are pronounced at the turning points. Both sound speeds were expressed in dimensionless variables and the parameters in the Munk profile were changed for simplicity to $\varepsilon = 0.01$, $d = 1.3\text{km}$ and $d = 1.5\text{km/s}$.

An embedded Runge-Kutta procedure with extrapolation and step-size control/prediction was used to integrate the system in all four cases. This choice was made to take advantage of the explicit truncation error provided by the output of the embedded procedure. Error control was achieved by placing a constraint of 10^{-6} on all variables in the array, including momentum. This corresponds to an error of roughly $\sim 1\mu\text{s}$ in time and $\sim 1\text{mm}$ in distance. The null condition was evaluated at each step to gauge the relative success of regulating truncation error, rather than imposing a tolerance on the constraints of the system. In all cases the magnitude of the error in light cone placement $ds = 0$ was bound from above by $\sim 10^{-5}$, and in most cases by $\sim 10^{-6}$. Caustics, surface and bottom hits, as well as potential detector interactions were identified by a change in sign of an appropriate quantity, i.e. caustics were located by a change in sign of Y . The location was obtained by the method of false position.

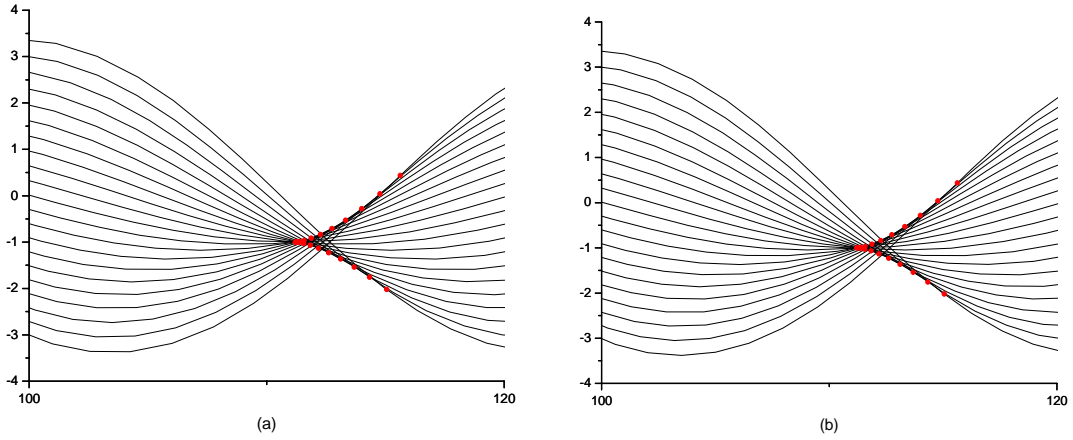


Figure 5. Detail of caustic for $\tilde{c} = 1 + 0.01\xi^2$: (a) range parameterized and (b) arc-length parameterized.

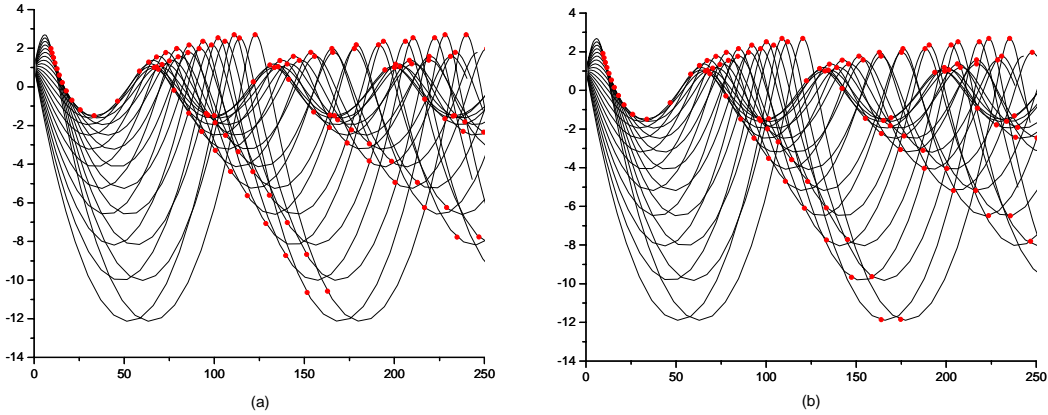


Figure 6. Sample ray trace for Munk profile: (a) affine parameterized and (b) time parameterized.

4. EXAMPLES

In this section several examples having exact solutions to the ray equations and the Jacobi equation in terms of ordinary functions are presented and discussed. Many of the cases presented here may be found in the literature^{13,17,21,31} and have been included here to shed light on the techniques outlined in Section 2. The approach presented here makes explicit use of the paraxial equations, Eqs. (3) and (28), with attention paid to the prediction of caustic curves from zeros of the Jacobi field, and interpreting the stability of neighboring rays by mapping divergence and convergence zones based on the sectional curvature.

In principle one knows $Y(\Lambda)$. The caustic is the locus of points determined by $Y = 0$. Solving this equation gives $\Lambda_c(\alpha)$, the value of the ray parameter at the caustic location in terms of the ray initial conditions. Using the ray coordinates then gives the caustic curve in space $x_c(\alpha)$, $z_c(\alpha)$, parameterized by the initial conditions of the ray. Cusps are determined by finding values of α for which the velocity of the caustic curve vanishes:

$$\frac{dx_c}{d\alpha} = \frac{dz_c}{d\alpha} = 0. \quad (45)$$

A few simple cases are analyzed from the differential geometric point of view. The simplest cases are well known examples that provide more insight into the language of differential geometry. Afterwards less trivial cases are presented, with solutions to the caustic curves determined by the geodesic deviation equation.

4.1 Layered Media with Smooth $c(z)$ and $v(z)$

The first two examples illustrate the differences in using λ and time as affine parameters. Both cases are described by stationary media, and the conformal metric introduced earlier is used. Recall from Section 3.2 that for purely two-dimensional systems, the sectional curvature is $K = c\nabla^2 c - \bar{\nabla}c \cdot \bar{\nabla}c$. For simplicity consider rays in the x - z plane. Along any ray an orthonormal basis may be constructed by inspection consisting of the unit tangent vector along the ray $\bar{t} = \dot{x}\hat{i} + \dot{z}\hat{k}$ and two basis vectors, the first being obtained by rotation of the ray tangent by 90 degrees, $\hat{e}_1 = -\dot{z}\hat{i} + \dot{x}\hat{k}$, the other being $\hat{e}_2 = \hat{j}$. In the conformal metric, coordinate time is a proper affine parameter and “dot” refers to differentiation with respect to time. The basis vectors (\hat{e}_1, \hat{e}_2) are orthonormal with respect to the conformal inner product $g_{ij} = \delta_{ij} / c^2$. The sectional curvature in the $\langle \bar{t}, \hat{e}_1 \rangle$ plane is $K = cc'' - (c')^2$, while the sectional curvature in the $\langle \bar{t}, \hat{e}_2 \rangle$ plane vanishes. From these results it follows that rays fired from a point source at the same initial angle but in different planes will diverge linearly in time.

Spherical Geometry and Ideal Focusing

By direct calculation the sound-speed profile $c(z) = C \cosh(\sqrt{K_0} z / C)$ produces a space of constant positive curvature $K = K_0$. The deviation vector can be solved exactly for all rays in this system: $Y(t) = A \cos(\sqrt{K}t) + B \sin(\sqrt{K}t)$. One can conclude from this that ideal periodic focusing will occur along each and every ray with the same frequency regardless of the placement of the source. The time-versus-depth integral can be calculated in this case leading to the result that the travel time between turning points is independent of initial conditions, hence the point-like focusing demonstrated in this case

will always occur³¹. In the affine representation the sectional curvature is $K = \alpha^2 K_0$. The appearance of the ray parameter leads to a nontrivial change in the interpretation of the geometry of space and its effect on geodesics.

With time parameterization, the geometry is identical to a two-dimensional sphere. The periodic ray structure can be mapped into a sphere by morphing the rays in such a way that they resemble those of a source placed on the waveguide axis, then identifying consecutive focal points with the north and south poles of the sphere. The rest of the space is then projected stereographically onto the sphere. The resulting space, while being geometrically identical to a sphere, is topologically equivalent to a sphere with two holes pinched in it identified with $z = \pm\infty$.

With affine parameterization, the geometry is spherical along each ray with a different effective radius of curvature for each value of α . Rays fired towards $z = \pm\infty$ never turn and their neighbors drift away from them at a constant rate. In the previous case all rays experience the same curvature, indicating that even those fired towards $z = \pm\infty$ converge with their neighbors passing through caustics. It can be easily verified by direct calculation of the ray integrals that the total travel time from $-\infty$ to $+\infty$ is equal to the period between consecutive conjugate points. Hence for a source placed anywhere in the space, the vertical rays meet the end of their journeys before ever encountering their neighbors. The finite travel time from $-\infty$ to $+\infty$ is an indication that the space described in the first case suffers from geodesic incompleteness¹³.

The Pseudosphere

The exact ray paths for the sound speed $c(z) = a + bz$ are circular arcs. The induced metric space is known in the literature as a Lobashevsky space and is an example of a space of constant negative curvature, or pseudosphere, $K = -b^2$. The deviation vector in this case may be found by inspection: $Y(t) = A \cosh(bt) + B \sinh(bt)$, implying that the distance between neighboring rays grows exponentially in time. Once again the affine version of the theory predicts a slightly different result. The curvature in this case is identically zero indicating that rays diverge linearly in λ .

Harmonic Waveguide

The harmonic waveguide, described by $n^2 = a + bz^2$, has been the subject of many studies due to the existence of exact solutions with nontrivial behavior for the rays and modes associated with this profile³⁰. Consider the special case $c^{-1} = \sqrt{1 - (1 - z)^2}$, with the units of speed scaled to 1. This sound speed forms a waveguide with symmetry axis at $z = 1$ and $c \rightarrow \infty$ at $z = 0$ and $z = 2$. The exact ray paths are sinusoidal:

$$z = 1 + \sqrt{1 - p^2} \sin(\Lambda + \varphi_0), \quad x = p\Lambda, \quad \sin \varphi_0 = \frac{z_0 - 1}{\sqrt{1 - p^2}}. \quad (46)$$

Consider a point source placed on the waveguide axis, $z = 1$. The sectional curvature is positive definite, the corresponding Jacobi field is

$$Y = \frac{p^2 \sin \Lambda + (1 - p^2) \Lambda \cos \Lambda}{\sqrt{1 - (1 - p^2) \sin^2 \Lambda}}. \quad (47)$$

For the special cases $p = 1$ and $p = 0$, $Y = \sin \Lambda$ and $Y = \Lambda$, respectively, as expected. The caustic is determined by solving the transcendental equation

$$\tan \Lambda = -\frac{1 - p^2}{p^2} \Lambda. \quad (48)$$

A plot of the rays and the caustics for a source on the symmetry axis is given in Fig. 7.

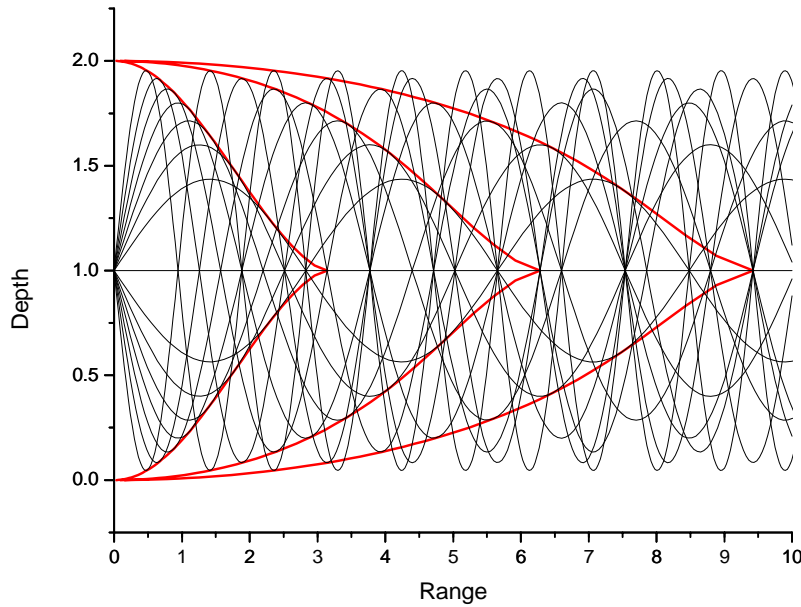


Figure 7. Ray fan and caustic structure for the n^2 quadratic sound-speed profile. The rays are plotted for even increments of $\cos \theta_0$. The caustics are traced by inserting solutions to Eq. (48) into Eq. (46).

The next few cases involve fluid motion. Very few interesting cases with exact solutions exist. We consider first the curvature induced by a class of symmetric velocity profiles that are found to create ducted regions. These ducts are identified by mapping the regions of positive sectional curvature into the x - z plane. Afterwards, the exact ray paths are presented for two special cases with nontrivial sound speed and fluid velocity.

Wind-Induced Sound Ducts

In general, effects of ν'' on a ray system are illustrated for a class of velocity functions of the form $\nu(z) = c_0(z/L)^{2n}$, where c_0 is the local sound speed, assumed to be a constant L , a length scale chosen such that the flow becomes supersonic for $|z| > L$ and $n > 0$ is a positive integer. This class of functions has the following common properties: $\nu(z)$ is a monotonically increasing function for $z > 0$, $\nu(z) \geq 0$ for all z , $\nu'(z) > 0$ for $z > 0$, $\nu''(z) > 0$ for all z , and $\nu(-z) = \nu(z)$. For the time being attention will be paid to rays that remain in regions of subsonic flow.

From Snell's Law, $\varepsilon(z) + \sec \theta = \varepsilon_0 + \sec \theta_0$, where ε_0 and θ_0 are the Mach number and initial angle of inclination at the source point, respectively. For purposes of illustration it is assumed that the source is placed at $z = 0$ and attention focused on rays fired in the upper half plane. For rays fired against the wind, $\theta_0 > \pi/2$ and $\sec \theta_0 < -1$. Combined with Snell's law this information implies that $\sec \theta < 0$ at all points along the ray, indicating that rays with a negative ray parameter will never turn back toward the source. On the other hand rays with positive ray parameter will always encounter vertical turning points, and because of the symmetry of $\nu(z)$ this will happen periodically.

The vertical turning points may be found from Snell's law by setting $\theta = 0$ and solving for z . Although the form of Snell's law used here is expressed in terms of the direction of the wavefront normal, the geometry of the rays indicates that $\theta = 0$ when the ray encounters a vertical turning point. The equation for the turning points becomes $\varepsilon(z) = -1 + \sec \theta_0$. The condition $2 > \sec \theta_0 \Rightarrow \theta_0 < \pi/3$ is imposed to single out rays that turn before entering supersonic regions, a condition that holds for any choice of ν . The sectional curvature for this class of problems is

$$K = \frac{\kappa_0^2}{L^2 c_0^2} 2n(4n-1) \zeta^{2n-2} \cos \theta_0 \left(\frac{\cos \theta_0}{\cos \theta} - \frac{2n}{4n-1} \right) \quad (49)$$

for all rays in the system, where the dimensionless variable $\zeta \equiv z/L$ is used. Clearly the sign of K depends on two factors, $\cos \theta_0$ and the term in parenthesis. Equation (49) will change sign when $\cos \theta = \cos \theta_0 (2 - 1/2n)$, the same result holding for rays fired both into and against the wind. Since $\cos \theta$ is an increasing function along rays with $\cos \theta_0 < 0$, the condition is never satisfied and these rays will remain in a divergence zone forever. Rays with $\cos \theta_0 > 0$ are a little more interesting. The curvature will remain positive along these rays only if $\cos \theta < \cos \theta_0 (2 - 1/2n)$. Since ν is strictly increasing $\cos \theta$ is strictly increasing as well and it suffices to check the curvature at the turning point where $\cos \theta = 1$. The curvature will be zero at the turning point if $\cos \theta_0 = 2n/(4n-1)$. For $n = 1$ this leads to the constraint $\cos \theta_0 = 2/3$, or $\theta_0 \approx 48^\circ$. Rays fired into the wind with $\cos \theta_0 > 2/3$ will remain in a region of positive curvature

as they propagate downstream. Rays with $\cos \theta_0 < 2/3$ will start with $K > 0$ and eventually along the ray $K \leq 0$, causing neighboring rays to begin diverging with respect to λ , in general when $\cos \theta = 2n \cos \theta_0 / (4n - 1)$. Figure 8 shows the convergence and divergence zones for a point source placed on the waveguide axis. The zones are labeled by the sign of the sectional curvature, K .

In the case $n = 1$, the ray equations and the deviation equation may all be integrated between turning points to yield solutions for the time of flight, range, and deviation vector as functions of depth in terms of elliptic functions. A ray trace using the same technique employed in Section 3 is shown below along for one half of a ray fan, with the placement of the caustics along each ray shown in the detail (Fig. 9). The procedure was stable with an upper bound on the deviations from the null surface $\sim 10^{-4}$ for the same truncation-error tolerance. Figure 8 shows the regions of positive and negative curvature mapped in the x - z plane for a source at the origin. There is a cut-off for rays fired with the wind at $p = 2/3$, $z = 1/\sqrt{2}$. Rays with $p > 2/3$ have turning points at $z < 1/\sqrt{2}$ and remain completely within a region in positive curvature.

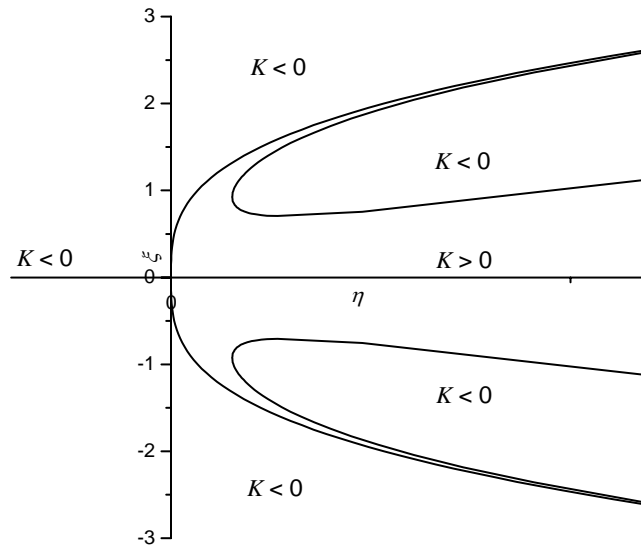


Figure 8. Convergence and divergence zones for the quadratic fluid-velocity profile. Regions are marked according to the sign of K . The outer $K = 0$ boundary corresponds to the $\alpha = 0$. The inner boundaries correspond to a source placed at the origin, on the symmetry axis of the guide.

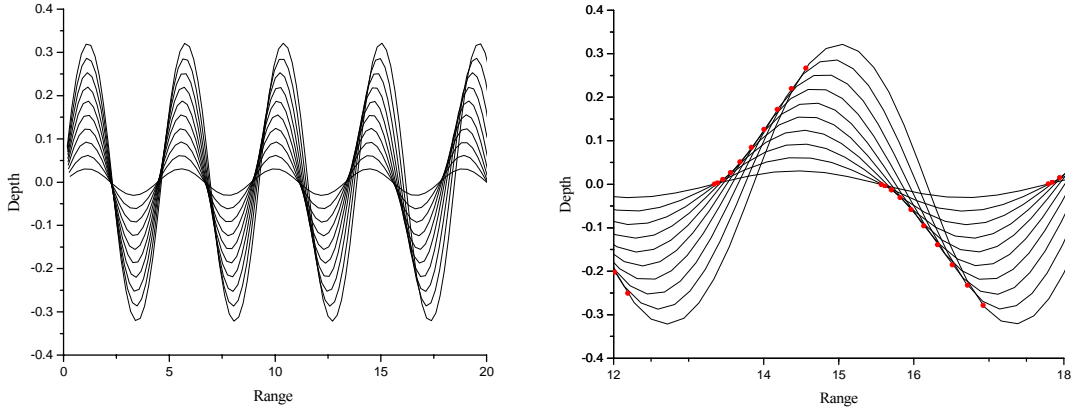


Figure 9. Ray trace for (left) the quadratic wind profile, with detail (right) for one cycle of the ray-path motion illustrating caustic formation.

Linear Fluid Velocity

For a linear fluid-velocity profile, $v = cz/L$, $c = \text{constant}$, and $K = -\kappa_1^2/L^2$. The deviation equation may be integrated to yield

$$Y = (\dot{Y}_0/\sqrt{K})\sinh(\sqrt{K}\lambda) + Y_0 \cosh(\sqrt{K}\lambda). \quad (50)$$

Hence neighboring rays with the same initial position will diverge at a rate of $Y = (\dot{Y}_0/\sqrt{K})\sinh(a\kappa_1\lambda/c)$ with respect to the affine parameter. The ray coordinates may also be solved in this case. Defining new dimensionless variables along the ray $\zeta \equiv \alpha(c\xi) - 1$, $\xi \equiv z/L$, $\tau \equiv c^2\alpha t/L$, $\eta \equiv x/L$, $\sigma \equiv \alpha\lambda/L$, and the new ray parameter $\beta \equiv c\alpha$, Eqs. (21)-(23) may be integrated to yield

$$\zeta = \beta \cosh(\sigma - \varphi) \quad (51)$$

$$\tau = \beta \sinh(\sigma - \varphi) - A_0 \quad (52)$$

$$\xi = \xi_0 + \frac{1}{2} \ln A_0 + \frac{1}{2} \sigma - \frac{1}{\beta} (2 - \beta \cosh(\sigma - \varphi)) \sinh(\sigma - \varphi), \quad (53)$$

where the parameters $A_0 \equiv \sqrt{\zeta_0^2 - \beta^2} + \zeta_0$ and $\varphi \equiv \ln(\beta/A_0)$ have been defined. Eqs. (51)-(53) represent the affine-parameterized coordinates for a segment of the ray with $\dot{z} > 0$ and the initial conditions set so that $\tau(0) = 0$. The ray-path geometry implied by these equations is well known¹³:

$$\eta = \eta_0 + \frac{1}{2} \ln \left(\frac{(1 - \alpha\xi) - \sqrt{(1 - \alpha\xi)^2 - \alpha^2}}{(1 - \alpha\xi_0) - \sqrt{(1 - \alpha\xi_0)^2 - \alpha^2}} \right) - \frac{1}{2\alpha^2} \left((1 - \alpha\xi) \sqrt{(1 - \alpha\xi)^2 - \alpha^2} - (1 - \alpha\xi_0) \sqrt{(1 - \alpha\xi_0)^2 - \alpha^2} \right) . \quad (54)$$

Equation (54) gives the upward part of the ray while the downward portion is determined by symmetry to be $2\eta_p - \eta$; η_0, ξ_0 are the initial coordinates of the ray and η_p, ξ_p are the coordinates of the turning point.

Linear Fluid-Velocity and Sound-Speed Profiles

Generalizing the last case, we consider the case $v = \xi$ and $c = 1 + \varepsilon\xi$. The exact ray paths are

$$\Lambda = - \left[\frac{\varepsilon}{\alpha^2(\varepsilon^2 - 1)} \sqrt{(1 - \alpha v)^2 - \alpha^2 c^2} + \frac{2}{\alpha^2(\varepsilon^2 - 1)^{3/2}} \arctan \left(\frac{(1 - \alpha v) + c \alpha \varepsilon}{\sqrt{(1 - \alpha v)^2 - \alpha^2 c^2} \sqrt{\varepsilon^2 - 1}} \right) \right]_{-\xi_0}^{\xi} ,$$

$$\tau = - \left[\frac{1}{\varepsilon^2 \sqrt{\varepsilon^2 - 1}} \arctan \left(\frac{(1 - \alpha v) + c \alpha \varepsilon}{\sqrt{(1 - \alpha v)^2 - \alpha^2 c^2} \sqrt{\varepsilon^2 - 1}} \right) + \frac{1}{\varepsilon^2} \ln \left(2(\alpha + \varepsilon) \frac{(1 - \alpha v) + \sqrt{(1 - \alpha v)^2 - \alpha^2 c^2}}{c} \right) \right]_{-\xi_0}^{\xi} ,$$

$$\eta = -\tau - \left[\frac{1}{\alpha \varepsilon} \sqrt{(1 - \alpha v)^2 - \alpha^2 c^2} \right]_{-\xi_0}^{\xi} , \quad (55)$$

while the Jacobi field along the ray as a function of depth is

$$y = \frac{c_1(1 - \alpha v)}{\alpha^2(\alpha + \varepsilon)} + c_2 \sqrt{(1 - \alpha v)^2 - \alpha^2 c^2} . \quad (56)$$

The sectional curvature is $K = -\alpha(\alpha + \varepsilon)/c^3$. In this case the curvature is negative for rays fired with the wind, $\alpha > 0$, indicating divergent behavior. For rays fired against the wind the sign on the curvature depends on the sign of $(\alpha + \varepsilon)$. Setting $(\alpha + \varepsilon) = 0$ implies $\cos\theta_0 = -\varepsilon$. For $\varepsilon > 1$ the fluid motion is always subsonic and a change in sign of K for rays fired against the wind is not possible, while for $1 > \varepsilon > 0$ fluid flow

becomes supersonic at $z = 1/(1 - \varepsilon)$, $K > 0$ when $|\cos \theta_0| < \varepsilon$ and $K < 0$ when $|\cos \theta_0| > \varepsilon$. The curve defined by $\alpha = 0$ is

$$\eta_{\alpha=0} = \frac{\xi - \xi_0}{\varepsilon} - \frac{1}{\varepsilon^2} \ln \left(\frac{1 + \varepsilon \xi}{1 + \varepsilon \xi_0} \right), \quad (57)$$

and the curve defined by $\alpha = -\varepsilon$ when $1 > \varepsilon > 0$ is

$$\eta_{\alpha=-\varepsilon} = \frac{\sqrt{1 - \varepsilon^2}}{\varepsilon} (\xi - \xi_0) - \frac{1}{\varepsilon^2 \sqrt{1 - \varepsilon^2}} \ln \left(\frac{1 + \varepsilon \xi}{1 + \varepsilon \xi_0} \right). \quad (58)$$

A plot of the convergence zones for each case is given in Fig. 10.

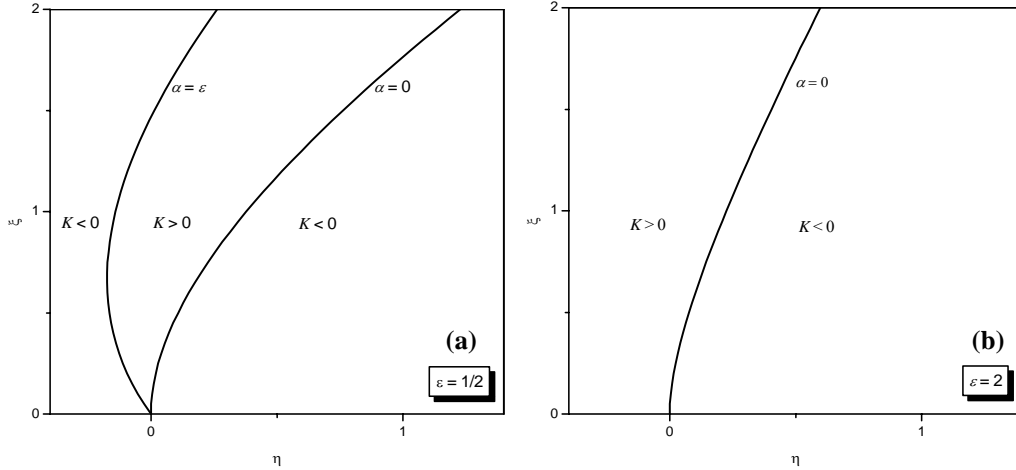


Figure 10. Convergence and divergence zones for the c -linear, D -linear case outlined above. (a) corresponds to $\varepsilon = 0.5$ and is sound-speed dominated with subsonic flow, while in case (b) $\varepsilon = 2$, with supersonic flow occurring at $\xi = 1$.

4.2 Piecewise-Linear Profiles

Although the linear sound-speed and fluid-velocity profiles lead to ray systems with somewhat benign behavior, they are frequently used to formulate exact ray theoretical models of real situations where the sound-speed and velocity profiles are approximated by piecewise-linear functions. In such cases the ray paths and their first derivatives are continuous and exact solutions to the ray path and the Jacobi field are known in each piecewise-linear region. The discontinuity in the sound-speed and velocity gradients

leads to the presence of a Dirac delta function in the sectional curvature, in turn leading to special boundary conditions for matching the Jacobi fields of different segments at the boundary between two regions. The basic situation is illustrated in Fig. 11. The medium is divided in depth into a finite number of regions. As a ray travels through the medium it will turn and periodically encounter each region, in principle an indefinite number of times. The ray segments are indexed in order of increasing ray parameter without reference to the corresponding region. The Jacobi field is a function of the affine parameter evaluated along the ray path. Each ray segment in space corresponds to an increment of the affine parameter. Passing from one region to another in space corresponds to boundary point along the Λ axis—see Fig. 12.

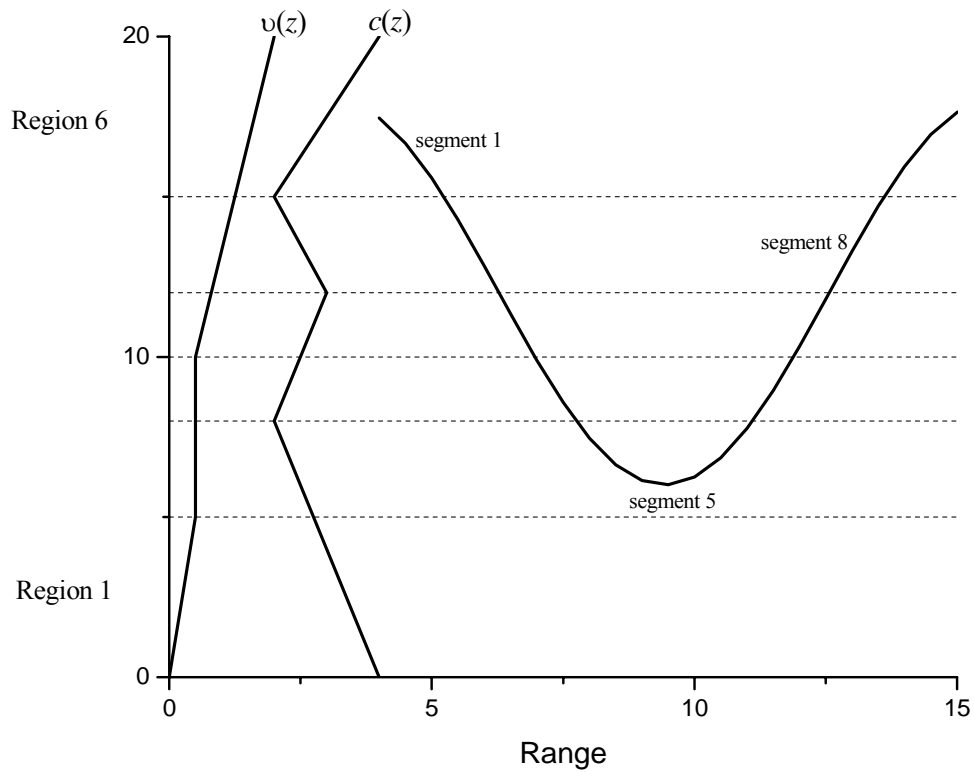


Figure 11. A physical situation approximated by piecewise-linear sound-speed and fluid-velocity profiles. A sample ray is drawn illustrating the meaning of the index labels along the ray as well as those labeling the different regions.

Once the rays are matched up, the parameter value, time of flight, and range for each segment may be determined. The Jacobi field is continuous leading to the boundary condition $Y_{i+1} = Y_i$. Integrating Eq. (26) across a boundary leads to the following condition on the discontinuity in \dot{Y} :

$$\dot{Y}_{i+1}(\Lambda_B) - \dot{Y}_i(\Lambda_B) + QY_i(\Lambda_B) = 0, \quad (59)$$

$$Q = \frac{1}{\dot{z}_B c_B^2} (\alpha \Delta v' (1 - \alpha v_B) + \alpha^2 c_B \Delta c'), \quad (60)$$

where the subscript B means evaluated at the boundary and $\Delta v'$, $\Delta c'$ are the discontinuities in the fluid velocity and sound speed, respectively, at the boundary. Once these conditions are matched for a significant number of segments the caustics and their features are determined in the same manner as before. A striking feature of these models is that nontrivial focusing emerges as a result of the boundary conditions, exclusively the curvature being otherwise zero or negative. In general the rays and the Jacobi field in each region are given by Eqs. (55) and (56) of the last section with appropriate changes in scale of the coordinates.

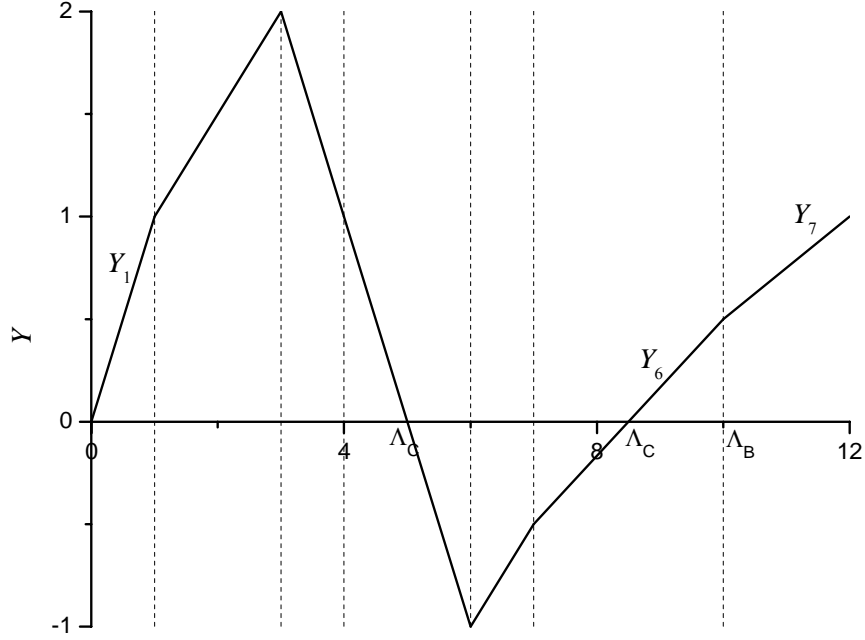


Figure 12. The Jacobi field for the profile illustrated in Fig. 11. The individual segments of Y shown here are linear merely for simplicity. The different depth regions in Fig. 11 correspond to intervals on the Λ axis. Comparing Figs. 12 and 11 indicates, for example, that the 4th and 6th intervals in Fig. 12 both correspond to region 3 of Fig. 11.

Two special cases of interest are: (1) a stationary medium with a piecewise-linear sound speed and (2) constant sound speed with a piecewise-linear fluid velocity. In case 1 the curvature is identically zero in each region and the Jacobi field may be written $Y_i = A_i + B_i \Lambda$, while in case 2 the curvature is a negative constant in each region and the

Jacobi field is $Y_i = A_i e^{\sqrt{-K}\Lambda} + B_i e^{-\sqrt{-K}\Lambda}$. In each case applying boundary conditions on Y leads to expressions for the coefficients A and B in terms of the ray parameter p and the source coordinates. The caustic in each region is determined by the condition $Y_i = 0$ leading to Λ_{iC} , with $\Lambda_{iC} = -A_i/B_i$ in case 1 and $2\sqrt{-K}\Lambda_{iC} = \ln(-B_i/A_i)$ in case 2, for the value of affine parameter along the i -th segment of the ray at which the caustic occurs. Inserting this expression into the appropriate ray equation then gives the caustic coordinates along the ray as a function of initial conditions. The piecewise-linear profiles give rise to cusp and broken caustics depending on the relative values of the profile slopes in consecutive regions. Two cases utilizing this procedure are illustrated next. Both cases involve stationary media due to their simplicity and past use in underwater acoustic modeling. The generalization to non-stationary media based on the steps outlined above is immediate.

Sound Incident on a Linear Half Space

This classic problem of sound in a homogeneous medium incident on a region of space with a graded refractive index is known to produce a caustic in the emerging field³¹, and in the graded medium. In affine parameterization, the equations for the ray path are

$$\frac{dx}{d\lambda} = \alpha, \quad \frac{dt}{d\lambda} = \frac{1}{c^2}, \quad \frac{dz}{d\lambda} = \pm \frac{\sqrt{1 - \alpha^2 c^2}}{c}, \quad (61)$$

with the local sound speed given by $c(z) = c_0\Theta(z) + c_0(1 - z/L)\Theta(-z)$, where $\Theta(z)$ is the Heaviside-step function and the dimensions of λ are L^2/T . Defining $\cos\theta_0 = p$ the rays in region $z > 0$ are straight lines given by

$$\eta = p\Lambda + \eta_0, \quad \xi = \xi_0 \pm \sqrt{1 - p^2}\Lambda, \quad \tau = \Lambda + \tau_0. \quad (62)$$

Here we define the dimensionless variables $\Lambda \equiv \lambda/Lc_0$, $\xi \equiv z/L$, $\eta \equiv x/L$, and $\tau \equiv tc_0/L$. For simplicity we set $\tau_0 = 0$ and consider a source placed at $\eta_0 = 0$ and $\xi_0 > 0$. Furthermore, we focus attention on rays with $\sin\theta_0 < 0$. The solution of the ray equations in the linear region may be expressed as

$$\left(\eta - \left(\eta_1 + p^{-1}\sqrt{1 - p^2}\right)\right)^2 + (\xi - 1)^2 = p^{-2}, \quad (63)$$

where $\eta_1 = \xi_0 \cot\theta_0$. The equation for η is the same in both regions. The ray paths in space are circles of radius $r = |\sec\theta_0|$ centered at $(\eta_1 + \tan\theta_0, 1)$. By symmetry the ray path emerges from region 2 at $-\theta_0$. Hence the third segment satisfies $\Delta z/\Delta x = -\tan\theta_0$.

At the second boundary point we have $\eta_2 = \xi_0 \cot \theta_0 + 2 \tan \theta_0$, leading to the following equation for ξ :

$$\xi(\Lambda) = \sqrt{1-p^2} \Lambda - (\xi_0 + 2(p^{-2} - 1)) . \quad (64)$$

The initial conditions on Y_1 are chosen to describe the geometry of neighboring rays from a point source, $Y_1 = \delta\theta \Lambda$. Applying the boundary conditions leads to the following recursion relation

$$Y_i(\Lambda) = Y_{i-1}(\Lambda) - \kappa Y_{i-1}(\Lambda_{i-1})(\Lambda - \Lambda_{i-1}), \quad i = 2, 3 , \quad (65)$$

for the solution along each segment of the ray path, with $\kappa = p^2 / \sqrt{1-p^2}$. Solving for the coefficients gives $A_2 = 1 - \kappa\Lambda_1$, $A_3 = -1$, $B_2 = \kappa\Lambda_1^2$, and $B_3 = 4\kappa^{-1}$, with

$$Y_2 = (1 - \kappa\Lambda_1)\Lambda + \kappa\Lambda_1^2, \quad Y_3 = -\Lambda + 4\kappa^{-1}, \quad (66)$$

for the Jacobi field in each region. An overall factor of $\delta\theta$ has been divided out for convenience. For a caustic to exist in the lower portion of the medium it is sufficient to require $Y_2(\Lambda_2) < 0$. This places the following constraint on the initial conditions of the ray path: $\xi_0 > 2(p^{-2} - 1)$. This condition implies two things depending on the question asked. First, for a given initial ray labeled p , at what location of the source does the caustic on that ray pop out (in) the lower half space? For $\xi_0 > 2(p^{-2} - 1)$, the caustic along ray p will be inside the lower region. Asked another way, for a fixed source location which rays pass through the caustic in region 1 and which in region 2? Solving for p in the inequality gives

$$p > \sqrt{\frac{2}{2 + \xi_0}} . \quad (67)$$

Rays fired at steep angles (small p) will penetrate deeply and pass through the caustic in the upper half space while those with shallow launch angles (large p) will pass through the caustic in the lower half space. These statements assume that the ray in question will pass through a caustic.

Along ray segment 3, we have $\Lambda_c = 4\kappa^{-1}$. Using the ray coordinates gives

$$\xi_c = 2(p^{-2} - 1) - \xi_0 , \quad \eta_c = 4\sqrt{p^{-2} - 1} , \quad (68)$$

or simply

$$\xi_c = \frac{\eta_c^2}{8} - \xi_0 \quad (69)$$

for the caustic curve in the upper half space. The caustic curve in the lower portion of space is more difficult to extract. For a caustic to form along segment 2 of the ray path we have $\Lambda_c = \kappa\Lambda_1^2/(\kappa\Lambda_1 - 1)$. To extract a curve $f(\xi_c, \eta_c) = 0$ for the caustic, independent of the initial conditions, requires solving the following equation for p :

$$(a^2 + b^2)p^6 - b(2b+1)p^4 + (2b+1)p^2 - 1 = 0, \quad (70)$$

where $b \equiv 1 + \xi_0$ and $a \equiv \xi_0^2/\eta_c$. The exact roots may be found by substituting $p^2 = q$ and solving the third-order equation. Rather than solve for $\xi_c(\eta_c)$ in region 2, we express the caustic as a parameterized curve $(\xi_c(p), \eta_c(p))$ for fixed ξ_0 :

$$\eta_c = \frac{p^3}{\sqrt{1-p^2}} \frac{\xi_0^2}{(\xi_0+1)p^2-1}, \quad (\xi-1)^2 = p^{-2} \left(1 - \frac{(1-p^2)^3}{((\xi_0+1)p^2-1)^2} \right). \quad (71)$$

The velocity of the caustic is

$$\frac{d\eta_c}{dp} = \xi_0^2 \frac{p^2(p^2(\xi_0+3)-3)}{(1-p^2)^{3/2}(p^2(\xi_0+1)-1)^2}, \quad (72)$$

$$\frac{d\xi_c}{dp} = \xi_0^2 \frac{p(p^2(\xi_0+3)-3)}{((\xi_0+1)p^2-1)^{5/2}(p^4+p^2(\xi_0^2+2\xi_0-2)+1-2\xi_0)}. \quad (73)$$

Clearly both vanish when $p = \sqrt{3/(\xi_0+3)}$ indicating the development of a cusp. This cusp will always exist in region 2 as long as $\xi_0 > 0$. Ray traces and caustics are shown for a few source placements in Fig. 13. The caustics, appearing on top of the ray trace, were derived from the solutions presented here. One can clearly see the development of the cusp in the lower half space. As the source is pulled up, the caustic sinks further down into the lower region with the cusp moving further away from the origin. The tail of the caustic approaches zero as $\eta_c \rightarrow \infty$. In the limiting case where the source is placed on the η axis, the cusp moves right up to the source and the tail merges with the η axis.

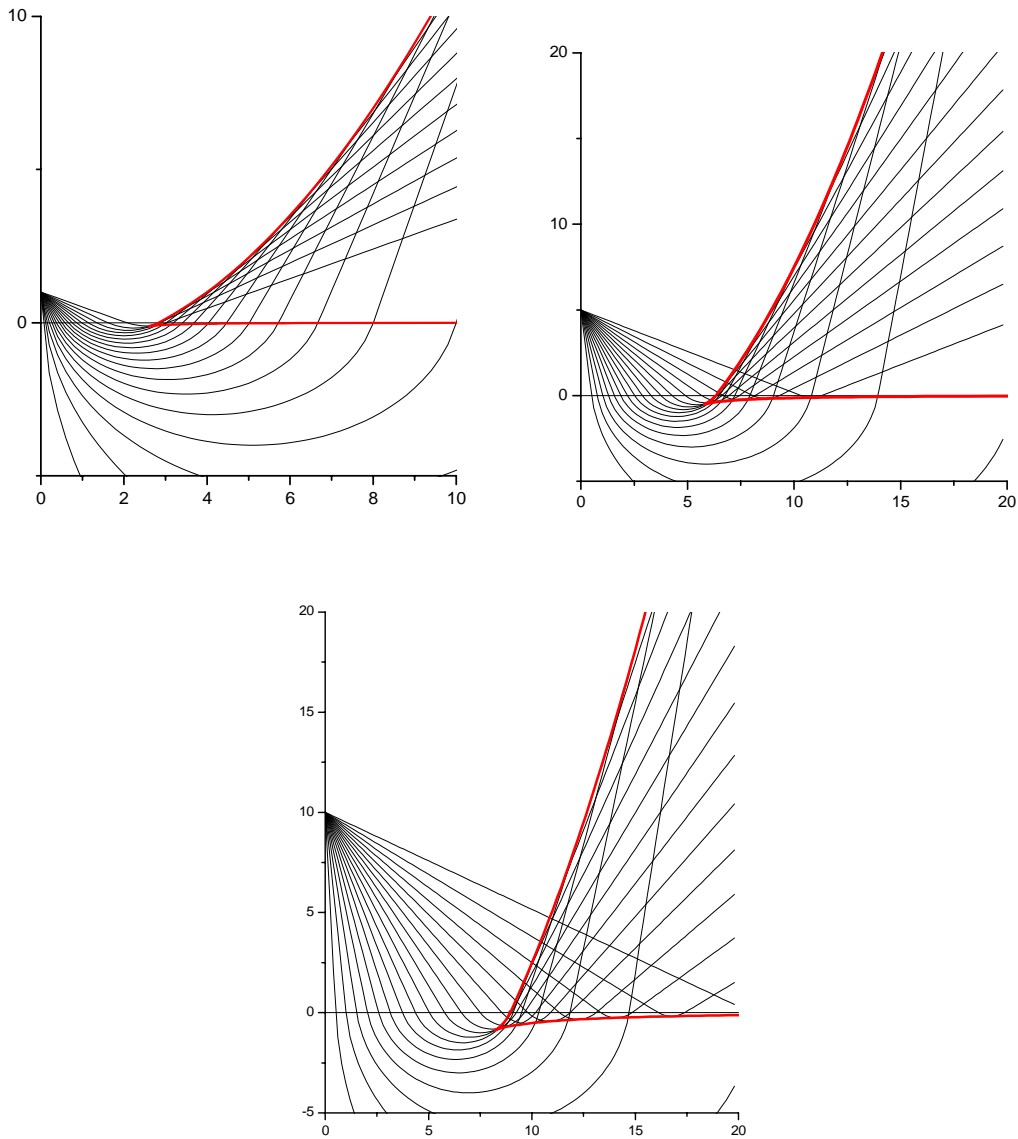


Figure 13. Ray fan incident on a c -linear half space for 3 source placements, from upper left going clockwise, $\xi = 1, 5,$ and 10 .

The Wedge Duct

Consider $\tilde{c}(\xi) = (1 + \xi)\Theta(\xi) + (1 - \sigma\xi)\Theta(-\xi)$ (Fig. 14). The upper portion of the duct is fixed at a 45-degree slope, while σ measures the steepness of the lower part of the duct relative to that of the upper part. For simplicity consider a source placed on the positive ξ axis. The initial ray parameter is $p = \cos\theta_0/(1 + \xi_0)$. The ray is divided into segments labeled γ_i . The points where the ray crosses the η axis are labeled η_i and the corresponding parameter value Λ_i . The first segment is given by

$$\left(\eta \mp p^{-1} \sqrt{1-p^2(1+\xi_0)^2}\right)^2 + (1+\xi)^2 = p^{-2}, \quad (74)$$

with a $-$ sign for rays fired upward and a $+$ sign for rays fired downward. After traversing this segment, the ray periodically crosses the η axis with the same value of ray parameter determined by Snell's law, $\cos \theta_1 = \cos \theta_0 / (1 + \xi_0)$. In region I the ray is

$$\left(\eta - \left(\eta_i + p^{-1} \sigma^{-1} \sqrt{1-p^2}\right)\right)^2 + (\sigma^{-1} - \xi)^2 = p^{-2} \sigma^{-2}, \quad (75)$$

while rays in region II are given by

$$\left(\eta - \left(\eta_i + p^{-1} \sqrt{1-p^2}\right)\right)^2 + (1+\xi)^2 = p^{-2}. \quad (76)$$

The crossing point of the first segment is $\eta_1 = p^{-1} \sqrt{1-p^2} \pm p^{-1} \sqrt{1-p^2(1+\xi_0)^2}$, and the crossing points for the other segments are

$$\eta_i = \eta_1 + (i(1+\sigma^{-1}) - 2) p^{-1} \sqrt{1-p^2}, \quad i = 2, 4, 6, \dots,$$

$$\eta_i = \eta_1 + (i-1)(1+\sigma^{-1}) p^{-1} \sqrt{1-p^2}, \quad i = 3, 5, 7, \dots,$$

for the lower and upper arcs, respectively. Applying boundary conditions leads to the following expressions for the coefficients A_i and B_i :

$$A_i = \begin{cases} 1 \pm (i-1)(1+\sigma^{-1})R & i = 1, 3, 5, \dots \\ -\sigma(1 \pm (i-1)(1+\sigma^{-1})R) & i = 2, 4, 6, \dots \end{cases}$$

$$B_i = \begin{cases} -\frac{(1+\sigma)}{\sigma\kappa} (i-1)(1 \pm (i-1)(1+\sigma^{-1})R + R^2) & i = 1, 3, 5, \dots \\ \frac{(1+\sigma)}{\kappa} ((i-1) \pm (i(i-2) + 2 + i(i-2)\sigma^{-1})R + (i-1)R^2) & i = 2, 4, 6, \dots \end{cases},$$

where, for simplicity, we have defined the ratio

$$R = \frac{\sqrt{1-p^2(1+\xi_0)^2}}{\sqrt{1-p^2}},$$

and $\kappa = p^2 / \sqrt{1-p^2}$ as before.

Sample rays for $\sigma = 5$ and $\xi_0 = 1$ are shown in Fig. 15 along with caustics. The caustics are plotted for $q \in [0.2, 0.9]$. For $q = 1$ the upper and lower caustics terminate at ranges of 4.15 and 2.08, respectively. Both become unbound as q approaches 0. The Jacobi field along the first three segments is displayed in Fig. 15 for the four rays in Fig. 16.

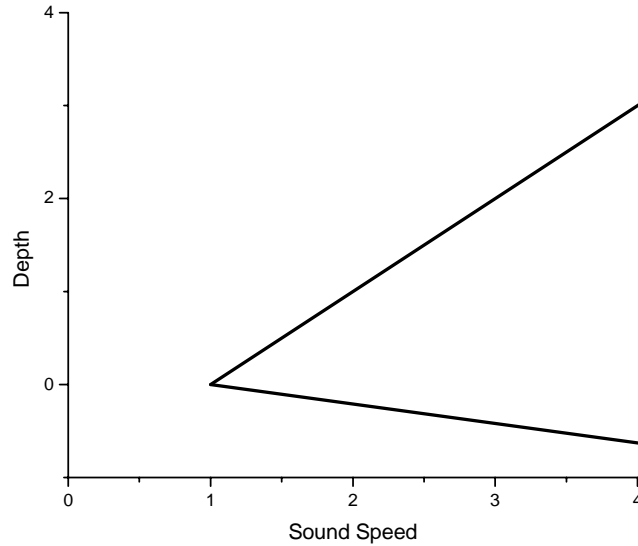


Figure 14. Sound-speed profile for the wedge duct. The lower portion is plotted for $\sigma = 5$.

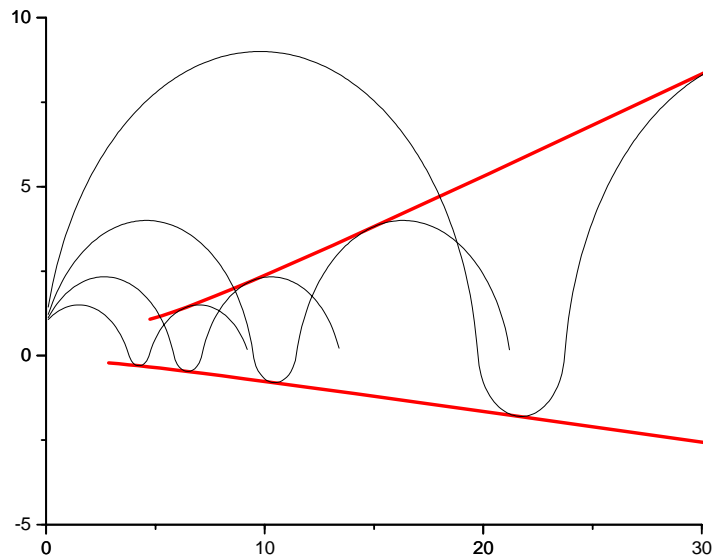


Figure 15. Caustic for the bilinear duct. Only 4 sample rays were traced for cleanliness.

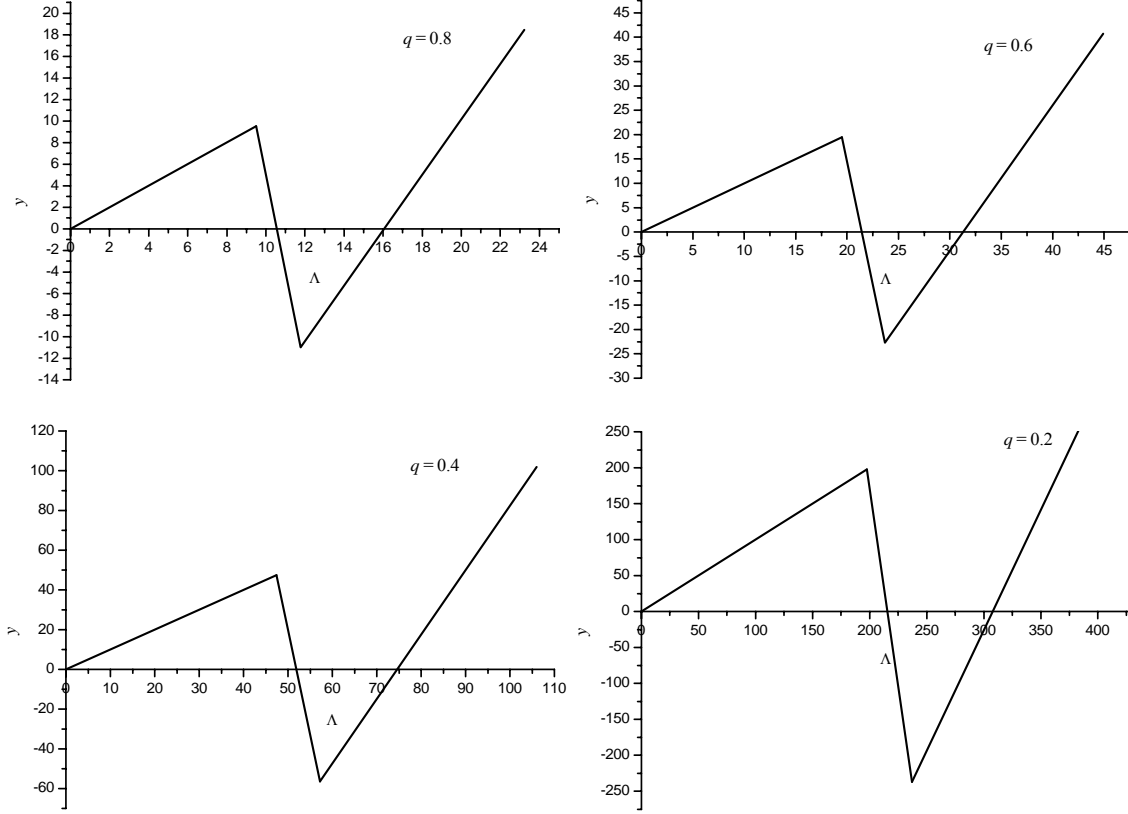


Figure 16. The Jacobi field plotted for the first 3 segments of 4 different rays, $\sigma = 5$ and $\xi_0 = 1$.

5. DISCUSSION AND CONCLUSION

The space-time dynamic ray-tracing procedure outlined in Section 1 provides a generalization to the approach currently used in seismology, and offers a method of beam tracing in a random medium. The identification of acoustic rays with null geodesics of a pseudo-Riemannian manifold leads immediately to this generalization. The geodesic deviation vector, used to model the deformation of an acoustic beam, allows one to measure geometric transmission loss and caustic location without repeatedly solving the ray equation. Additionally this identification has led to a continuum of theoretically equivalent paraxial ray-trace systems connected by conformal transformations, and points to a unified approach to extracting well-known results such as Snell's law and Fermat's principle in random fluid media. The null hypersurface is viewed as a manifold created by the local sound speed and fluid velocity which encodes all information about the acoustic field.

The development here was intended for describing acoustics in the presence of subsonic flow. This requirement is necessary for the identification of acoustic rays with null geodesics. For cases involving supersonic flow, the bicharacteristic condition defines the geometry of the acoustic rays as Euclidean line elements of zero length. Such spaces are a special case of a wider class called Finsler spaces. This identification indicates that these techniques may be generalized to include cases involving supersonic flow.

ACKNOWLEDGEMENTS

The work was performed under the Office of Naval Research / American Society for Engineering Education (ONR/ASEE) Summer Faculty Program. In addition to the ASEE, the author would like to thank the Naval Research Laboratory (NRL) in Washington, DC for hosting this fellowship for three summers (2002-2004), during which time some parts of this work were completed. The author would also like to acknowledge Dr. Daniel Wurmser, NRL, for helpful comments and discussions during the start of this project, and Dr. A. Lewis Licht, University of Illinois at Chicago, for bringing Matt Visser's article to his attention. Finally, thanks to Drs. Robert Gragg and Roger Gauss, NRL, for helpful discussions.

REFERENCES

1. W.G. Unruh, "Experimental black hole evaporation?," *Phys. Rev. Lett.* **46**, 1351-1353 (1981).
2. M. Visser, "Acoustic black holes: Horizons, ergospheres, and Hawking radiation," *Classical and Quantum Gravity* **15**, 1767-1791 (1998).
3. V. Cerveny, *Seismic Ray Theory* (Cambridge University Press, Cambridge, 2001).
4. R. Guenther, *Modern Optics* (John Wiley & Sons, New York, 1990). (Specifically, chapter 5, section entitled "Propagation in a Graded Index Optical Fiber", for a waveguide paraxial ray approximation.)
5. A. Abromowicz and W. Kluzniak, "Epicyclic Orbital Oscillations in Newton's and Einstein's Dynamics," *General Relativity and Gravitation* **35**, 69-77 (2003).
6. S.L. Bazanski, "Kinematics of relative motion of test particles in general relativity (1)," *Ann. Inst. Henri Poincare, Section A*, **XXVII**, 145-166 (1977).
7. C.W. Misner, K.S. Thorne, and J.A. Wheeler, *Gravitation* (Freeman, New York, 1973).

8. B. O'Neill, *Elementary Differential Geometry* (Academic Press, San Diego, 1966), Ch. VII.
9. P. Schneider, J. Ehlers, and E.E. Falco, *Gravitational Lenses*, Astronomy and Astrophysics Library (Springer-Verlag, New York, 1992).
10. R.M. Wald, *General Relativity* (The University of Chicago Press, Chicago, 1984).
11. M. Porter and H. Bucker, "Gaussian beam tracing for computing ocean acoustic fields," *J. Acoust. Soc. Am.* **82**, 1349-1359 (1987).
12. G.S. Heller, "Propagation of acoustic discontinuities in an inhomogeneous moving liquid medium," *J. Acoust. Soc. Am.* **25**, 950-951 (1953).
13. E.T. Kornhauser, "Ray theory for moving fluids," *J. Acoust. Soc. Am.* **25**, 945-949 (1953).
14. C. Perkeris, "Theory of propagation of sound in a half -space of variable sound speed under the condition of formation of a caustic," *J. Acoust. Soc. Am.* **18**, 295-315 (1946).
15. O.V. Rudenko, A.K. Sukhorukova, and A.P. Sukhorukov, "Full Solutions to the Equations of Geometrical Acoustics in Stratified Moving Media," *Acoustical Physics* **43**, 339-343 (1997).
16. R.J. Thompson, "Ray theory for an inhomogeneous moving medium," *J. Acoust. Soc. Am.* **51**, 1675-1682 (1972).
17. I. Tolstoy and C.S. Clay, *Ocean Acoustics, Theory and Experiment in Underwater Sound* (McGraw-Hill, New York, 1966).
18. P. Uginčius, "Acoustic-ray equations for a moving, inhomogeneous medium," *J. Acoust. Soc. Am.* **37**, 476-479 (1965).
19. P. Uginčius, "Ray acoustics and Fermat's principle in a moving inhomogeneous medium," *J. Acoust. Soc. Am.* **51**, 1759-1763 (1972).
20. R.W. White, "Acoustic ray tracing in moving inhomogeneous fluids," *J. Acoust. Soc. Am.* **53**, 1700-1704 (1973).
21. E.R. Franchi and M. Jacobson, "Ray propagation in a channel with depth-variable sound speed and current," *J. Acoust. Soc. Am.* **52**, 316-331 (1972).
22. R. Courant and D. Hilbert, *Methods of Mathematical Physics: Volume II* (John Wiley & Sons, New York, 1962).

23. F. John, *Partial Differential Equations* (Courant Institute of Mathematical Sciences Lecture Notes, New York University, New York, 1952).
24. S. Kobayashi and K. Nomizu, *Foundations of Differential Geometry: Volumes I and II* (John Wiley & Sons, New York, 1963). (*See Volume II, specifically Chapter VIII for a discussion of Jacobi fields and conjugate point theorems.*)
25. L.D. Landau and E.M. Lifshitz, *Fluid Mechanics, Second edition* (Butterworth & Heinemann, Oxford, 1987).
26. K. Smith, M. Brown, and F. Tappert, "Ray chaos in underwater acoustics," *J. Acoust. Soc. Am.* **91**, 1939-1949 (1992).
27. K. Smith, M. Brown, and F. Tappert, "Acoustic ray chaos induced by mesoscopic oceanic structure," *J. Acoust. Soc. Am.* **91**, 1950-1959 (1992).
28. H. Davis *et al.*, "The Hudson Laboratories Ray Tracing Program," Technical Report No. 150, Hudson Laboratories of Columbia University, 1968.
29. L.B. Palmer and D.M. Fromm, "The Range-Dependent Active System Performance Prediction Model (RASP)," NRL/FR/5160--92-9383, Naval Research Laboratory, Washington, DC, 1992.
30. T. Foreman, "A Frequency Dependent Ray Theory," Technical Report, ARL-TR-88-17, Applied Research Laboratories, The University of Texas at Austin, 1988.
31. L.M. Brekhovskikh, *Waves in Layered Media* (Academic Press, New York, 1960).
32. S.W. Hawking and G.F.R. Ellis, *The Large Scale Structure of Space-Time* (Cambridge University Press, Cambridge, 1973).

Appendix A

CONCEPTS FROM DIFFERENTIAL GEOMETRY

A.1 Metric

The metric is a generalization of the dot product and is usually introduced via a quadratic form

$$ds^2 = a_{ij} dx_i dx_j \quad , \quad (\text{A.1})$$

with ds a differential arc length and $a_{ij}(x_k)$ continuously differentiable functions of coordinates. One can always find a small neighborhood about an arbitrary point such that

$$a_{ij} \approx \text{diag}(\underbrace{1 \dots 1}_n \quad \underbrace{-1 \dots -1}_m) \quad , \quad (\text{A.2})$$

modulo constant scale factors, with $n + m = \dim(M)$.

When $m = 0$, the metric reduces to the identity matrix and the geometry is locally Euclidean. When $|n - m| = \dim(M) - 2$, the metric reduces to one of two choices for the Minkowski metric used in special relativity, specifically for $\dim(M) = 4$. Manifolds with metric defined by Eq. (A.1) that are locally Euclidean are referred to as Riemannian, while those that have local Minkowski geometry are termed either pseudo-Riemannian or Lorentzian.

A consequence of Eq. (A.2) is that curves on a pseudo-Riemannian manifold can have positive, negative, or zero length. The coordinates of the manifold are divided into x_i , $i = 1 \dots \dim(M) - 1$, and t , and choosing $m = 1$. With this convention, curves with $ds^2 > 0$ are called space-like, and curves with $ds^2 < 0$ time-like. These two types of curves are separated by a hypersurface defined by the class of curves with $ds^2 = 0$ referred to as a null hypersurface, a generalization of the light cone.

For subsonic flow, the metric introduced in Appendix B describes a Lorentzian manifold with $n = 3$ and $m = 1$. The characteristic condition identifies the acoustic rays with geodesic curves on the null hypersurface similar to photon trajectories in general relativity.

A.2 Manifolds

A manifold is an abstraction from the theory of surfaces that does not include a surrounding Euclidean space of higher dimension in its description. For a detailed definition of a manifold, see the References. We present here only a few concepts that are used in other places within the text. A tangent space, $T_p(M)$, is defined at each point on the manifold which serves as an abstraction of the tangent plane to a surface. Each tangent space has the structure of flat Euclidean space, modulo constant scale factors. The metric in each tangent space, $g_{\mu\nu}(x^\alpha)$, is fixed but is allowed to vary from point to point in M . If $U, V \in T_p(M)$ then their inner product is given by $g_{\mu\nu}U^\mu V^\nu$, and $g_{\mu\nu}V^\mu V^\nu \equiv \|V\|^2$ defines the magnitude of a vector. The V^μ are the components of the vector in some chosen basis of $T_p(M)$. A dual tangent space, $T_p^*(M)$, is also defined at each point of M . The metric tensor defines a mapping from $T_p(M) \rightarrow T_p^*(M)$, $T_\mu = g_{\mu\nu}T^\nu$. The T_μ are the components of the dual vector in some chosen basis of $T_p^*(M)$. Tensors of arbitrary rank are elements of a direct product space constructed of multiple copies of the tangent and dual tangent spaces $T_p(M) \times \dots \times T_p(M) \times T_p^*(M) \times \dots \times T_p^*(M)$. For example the metric presented in Section B.1 are components of a tensor in $T_p^* \times T_p^*$. These spaces do not require a concept of distance to be defined. In some sense defining a metric before this section is like putting the cart before the horse. The components of a tensor of arbitrary rank are denoted $T^{\alpha_1 \dots \alpha_N}_{\beta_1 \dots \beta_M}$. A standard choice of basis for $T_p(M)$ and $T_p^*(M)$ are ∂_μ and dx^μ respectively, where x^μ are coordinates defined on an open set of M containing p . In this basis a vector and its dual are denoted $V = V^\mu \partial_\mu$ and $V_\mu dx^\mu$, respectively.

A.3 Covariant Differentiation and Parallel Transport

The covariant derivative of a vector and dual vector are defined by

$$D_\mu U^\nu \equiv \partial_\mu U^\nu + \Gamma^\nu_{\mu\lambda} U^\lambda, \quad D_\mu U_\nu \equiv \partial_\mu U_\nu - \Gamma^\lambda_{\mu\nu} U_\lambda, \quad (\text{A.3})$$

respectively, where

$$\Gamma^\nu_{\mu\lambda} \equiv \frac{1}{2} g^{\nu\beta} \left(\partial_\mu g_{\lambda\beta} + \partial_\lambda g_{\mu\beta} - \partial_\beta g_{\mu\lambda} \right). \quad (\text{A.4})$$

These Christoffel symbols take into account the turning of the basis vectors as one differentiates the vector, requiring comparison of V at two points of M . Eq. (A.3) is a component form of the result.

Comparing vectors at different points in M is not a trivial operation since they live in different spaces. To compare $V \in T_p(M)$ to $V \in T_q(M)$, $p, q \in M$ with $p \neq q$, one of the vectors must be moved into the space of the other. In general this requires specifying the path in space, C , traversed by V from p to q . If T^μ is the velocity of C then V is parallel transported along C if

$$T^\mu D_\mu V^\nu = 0 \quad . \quad (\text{A.5})$$

A.4 Affine Parameter

Geodesic curves parallel transport their velocity vector, i.e.

$$\frac{DT^\nu}{d\lambda} = T^\mu D_\mu T^\nu = 0 \quad . \quad (\text{A.6})$$

When Eq. (A.6) holds the parameter λ defined along the curve is called an affine parameter. Any other choice of parameterization will change Eq. (A.6) to

$$T^\mu D_\mu T^\nu = \sigma T^\nu, \quad (\text{A.7})$$

where σ is an arbitrary scalar function defined along the curve. Equation (A.6) makes the transported tangent vector “parallel” to the tangent of the curve at the new point (allowing a change in magnitude), whereas the auto-parallel condition requires the transported tangent vector to be identical to the tangent vector at the new point along the curve. For space-like geodesics, arc length is an affine parameter. Time-like geodesics may also be parameterized by their length interpreted as a standard internal time, or the proper time of an observer whose world line coincides with the particular time-like curve. Clearly, for null curves arc length cannot be used as a parameter. In such cases one imposes Eq. (A.6) and the null constraint thus defining the parameter as affine with no physical significance attached.

A.5 Geodesics

Defined in the previous section as auto-parallel, the geodesic equation is also the Euler-Lagrange equation derived from a variation of the arc length,

$$\delta \int ds = 0 \quad , \quad (\text{A.8})$$

with ds defined in Appendix A.1. Equation (A.8) defines geodesics as curves of “optimal” length, either minimizing or maximizing the length between two points of M .

A.6 Curvature

The Riemann curvature tensor, and the covariant Riemann tensor are derived from the Christoffel symbols:

$$R^\mu{}_{\alpha\nu\beta} = \partial_\nu \Gamma^\mu{}_{\alpha\beta} - \partial_\beta \Gamma^\mu{}_{\alpha\nu} + \Gamma^\mu{}_{\lambda\nu} \Gamma^\lambda{}_{\alpha\beta} - \Gamma^\mu{}_{\lambda\beta} \Gamma^\lambda{}_{\alpha\nu}, \quad (\text{A.9})$$

$$R_{\mu\alpha\nu\beta} = \partial_\nu \{\mu; \alpha\beta\} - \partial_\beta \{\mu; \alpha\nu\} + \Gamma^\rho{}_{\alpha\nu} \{\rho; \mu\beta\} - \Gamma^\rho{}_{\alpha\beta} \{\rho; \mu\nu\}. \quad (\text{A.10})$$

The tensor defined in Eq. (A.10) has several symmetries that reduce the total number of components:

$$R_{\mu\nu\alpha\beta} = R_{\alpha\beta\mu\nu} = -R_{\nu\mu\alpha\beta} = -R_{\mu\nu\beta\alpha}.$$

The effects of curvature are most easily seen by parallel transporting a vector around a closed loop in M . If this task were attempted on a plane or in Euclidean space the result would be trivial, the transported vector would be identical to the original vector. A simple nontrivial example of parallel transport on a curved manifold is constructed by moving a vector from the north pole of a sphere around an equilateral geodesic triangle with $\theta = 90^\circ$. The transported vector is rotated by 90° relative to the old vector.

A.7 The Jacobi Equation

The geodesic equation gives curves of optimal length on M satisfying Eq. (A.5). The stability of a geodesic relative to slight variation in initial conditions is governed by the Jacobi equation. For convenience we define the Jacobi vector, Y , along the geodesic subject to the constraint $g_{\mu\nu} Y^\mu \dot{x}^\nu = 0$. Focusing exclusively on the null geodesics of M confines Y to the space-like plane $\langle e_I \rangle$. Geometrically Y points from one geodesic to a point on a neighboring geodesic with the same value of λ . The vector Y obeys a second-order linear differential equation along the geodesic:

$$\frac{d^2 Y_I}{d\lambda^2} + K_{IJ} Y_J = 0, \quad (\text{A.11})$$

which is derived from the second variation of the length integral. $Y_I = \hat{e}_I^\alpha g_{\alpha\beta} Y^\beta$ is the projection of Y onto the geodesic-centered frame field defined in Appendix C, and the curvature matrix $K_{IJ} \equiv R_{\mu\alpha\nu\beta} \dot{x}^\alpha \dot{x}^\beta \hat{e}_I^\mu \hat{e}_J^\nu$ is introduced. For $I = J$, K_{II} , no sum on I , is the sectional curvature in the plane spanned by $\langle \dot{x}, e_I \rangle$, and measures the relative rate of separation of neighboring geodesics.

Equation (A.11) governs the stability of the geodesics and provides a convenient paradigm for describing the focusing and spreading of a geodesic bundle in M . The

tendency for neighboring geodesic to converge or diverge is determined by the matrix K_{IJ} . If the curvature is positive definite in every plane containing the ray tangent, then neighboring rays from a common source point in all directions tend to converge and a three-dimensional ray bundle will focus. If the curvature is zero or negative everywhere along the ray, then neighboring rays from a common source point will tend to eventually diverge. (If $Y_0 \neq 0$ then the initial shape of the wavefront may cause the formation of a caustic independently of the focusing properties of the medium, as happens with light reflected from a concave surface in Euclidean space.) The conditions $K_{11} > 0$, and $\det K_{IJ} > 0$ along $\gamma(\lambda)$ are necessary and sufficient for the quadratic form $K_{IJ}Y_I Y_J$ to be positive definite.

A.8 Conjugate Points

Two points on a geodesic $\gamma(\lambda)$, P and Q , are said to be conjugate if there exists a nontrivial Jacobi vector along $\gamma(\lambda)$ that vanishes at P and Q . According to the conjugate-point theorems of differential geometry, if upper and lower bounds exist such that $k_1 \leq R(\hat{Y}, T, \hat{Y}, T) \leq k_2$ along some segment of the ray, then the period of affine parameter between consecutive conjugate points satisfies $\pi/\sqrt{k_2} \leq T \leq \pi/\sqrt{k_1}$. If the sectional curvature is zero or negative everywhere along $\gamma_F(\lambda)$, then neighboring rays will eventually diverge. (A single caustic may form if the initial region is concave but otherwise one does not expect the periodic development of focal points further downstream.) In situations where a ray occasionally may enter convergence and divergence zones, one cannot conclude from checking the Riemann tensor whether conjugate points will occur and how frequently.

Appendix B

NULL GEODESICS AND ACOUSTIC RAYS

This section introduces the connection between the null geodesics of a pseudo-Riemannian manifold and the bicharacteristics of the equations of hydrodynamics of ideal, isentropic fluids for the case of subsonic flow. The emergence of a geodesic structure from the study of hyperbolic partial differential equations is a hallmark of the method of characteristics. The same geodesic structure emerges in the study of acoustic rays, a connection that has been pointed out in the past by researchers in both the acoustics and relativity communities. In most cases one appeals to the high-frequency approximation although it should be pointed out that the same structure emerges in the general treatment of the system describing the propagation of discontinuities. The majority of this section contains little new information and is written for completeness, rigor and convenience, because the variety of different approaches has not been cataloged in one place. Every attempt at completeness is made while maintaining brevity.

B.1 The Bicharacteristics of the Equations of Hydrodynamics

The equations of hydrodynamics for ideal, isentropic fluids consists of the continuity equation and Euler's equation, respectively given by

$$\partial_t p + \bar{v} \cdot \bar{\nabla} p + \rho c^2 \bar{\nabla} \cdot \bar{v} = 0 \quad , \quad (\text{B.1a})$$

$$\partial_t \bar{v} + \bar{v} \cdot \bar{\nabla} \bar{v} + \frac{1}{\rho} \bar{\nabla} p + \bar{\nabla} \Phi = 0, \quad (\text{B.1b})$$

where p is the fluid pressure, \bar{v} the fluid velocity, ρ the fluid density, and where the fluid obeys an equation of state $\rho = \rho(p)$, with $\rho' = c^{-2}$ defining the local sound speed. The potential Φ is due to external forces such as gravity acting on the fluid. Equations (B.1a) and (B.1b) are a system of first-order quasi-linear partial differential equations. Applying the method of characteristics to this system leads to the characteristic matrix

$$\begin{bmatrix} D\varphi & \rho c^2 (\bar{\nabla} \varphi)^T \\ \rho^{-1} \bar{\nabla} \varphi & 1_{3 \times 3} D\varphi \end{bmatrix}, \quad (\text{B.2})$$

where the function $\varphi(\bar{x}, t)$ is the wavefront, defined as a surface in space-time on which the initial data of the fields are specified.

The characteristic conditions are satisfied by setting the determinant of the matrix equal to zero leading to

$$Q = (D\varphi)^2 \left((D\varphi)^2 - c^2 \bar{\nabla} \varphi \cdot \bar{\nabla} \varphi \right) = 0. \quad (\text{B.3})$$

Each term in Eq. (B.3) defines a partial Hamiltonian for the system and may be treated separately. Defining $H_1 = (D\varphi)^2$ and $H_2 = \left((D\varphi)^2 - c^2 \bar{\nabla} \varphi \cdot \bar{\nabla} \varphi \right)$, one set of characteristics is determined by

$$H_2 = g^{\mu\nu} \partial_\mu \varphi \partial_\nu \varphi = 0, \quad (\text{B.4})$$

where the contravariant metric tensor $g^{\mu\nu}$ has been introduced with $g^{00} = -c^{-2}$, $g^{0i} = -\mu_i$, $g^{ij} = \delta_{ij} - \mu_i \mu_j$, with $\bar{\mu} \equiv \bar{v}/c$ defining the local Mach number, or in matrix form

$$g^{\mu\nu} \equiv \frac{1}{c^2} \begin{pmatrix} -1 & -\nu_i \\ -\nu_j & c^2 \delta_{ji} - \nu_j \nu_i \end{pmatrix}. \quad (\text{B.5a})$$

The corresponding covariant metric tensor given by

$$g_{\mu\nu} = \begin{pmatrix} -c^2 + \nu^2 & -\nu_i \\ -\nu_j & \delta_{ji} \end{pmatrix} \quad (\text{B.5b})$$

is the inverse of Eq. (B.5a) satisfying $g_{\mu\alpha} g^{\alpha\nu} = \delta_\mu^\nu$. A factor of ρc^2 has been removed from Eq. (B.4) for simplicity but otherwise having no effect on the geometry of the curves defined by it. The bicharacteristics, which are identified with the curves along which energy is propagated, or with the rays of the system, are given by a set of trajectories in space-time. Defining an appropriate parameter λ along these curves and introducing the canonical momentum $p_\mu \equiv \partial_\mu \varphi$ in H_2 , the bicharacteristic equations are

$$\frac{dx^\mu}{d\lambda} = \frac{1}{2} \frac{\partial H_2}{\partial p_\mu} = g^{\mu\nu} p_\nu, \quad (\text{B.6a})$$

$$\frac{dp_\mu}{d\lambda} = -\frac{1}{2} \frac{\partial H_2}{\partial x^\mu} = -\frac{1}{2} p_\alpha p_\beta \partial_\mu g^{\alpha\beta}. \quad (\text{B.6b})$$

In Eq. (B.6b) the derivative of the contravariant metric can be replaced by the derivatives of the covariant metric by differentiating $g_{\mu\alpha} g^{\alpha\nu} = \delta_\mu^\nu$, thus combining Eqs. (B.6a) and (B.6b) leads to the following equation for the bicharacteristics:

$$\frac{d^2 x^\mu}{d\lambda^2} + \frac{1}{2} g^{\mu\nu} \{2\partial_\alpha g_{\nu\beta} - \partial_\nu g_{\alpha\beta}\} \frac{dx^\alpha}{d\lambda} \frac{dx^\beta}{d\lambda} = 0, \quad (\text{B.7})$$

which is precisely the equation for the geodesics of a differentiable manifold M with metric $g_{\mu\nu}$. From Eq. (B.7) and the characteristic condition, it follows that the bicharacteristic curves are equivalent to the null geodesics.

B.2 Linear Acoustics

To describe acoustics in the presence of background fluid motion, all fields in the problem are written in the form $\bar{v} = \bar{w} + \bar{v}$, $p = p_0 + p_1$, and $\rho = \rho_0 + \rho_1$, where \bar{w} , p_0 and ρ_0 are respectively the velocity, pressure and density of the fluid medium, and \bar{v} , p_1 and ρ_1 are contributions due to acoustic phenomena. In the following treatment of the problem it is assumed that the perturbations are weak, leading to a linear theory for the propagation of sound. No restriction is placed on the state equation for the background fluid motion, while the acoustic fluctuations are assumed to obey the adiabatic condition, $\rho_1 = c^{-2} p_1$. The background fields are assumed to obey the equations of hydrodynamics; with body forces such as gravity lumped together in the background equations, independently of the acoustic field. Applying these assumptions to Eqs. (B.1a) and (B.1b) gives

$$\{D^* p_1 + c^2 \rho_0 \bar{\nabla} \cdot \bar{v}\} + \{p_1 \bar{\nabla} \cdot \bar{w} + c^2 \bar{v} \cdot \bar{\nabla} \rho_0 + p_1 c^2 D^* c^{-2}\} = 0, \quad (\text{B.8a})$$

$$\{\rho_0 D^* \bar{v} + \bar{\nabla} p_1\} + \{c^{-2} p_1 D^* \bar{w} + \rho_0 \bar{v} \cdot \bar{\nabla} \bar{w}\} = 0, \quad (\text{B.8b})$$

for the acoustic perturbations, where $D^* \equiv \partial_t + \bar{w} \cdot \bar{\nabla}$, following Thompson's notation and the adiabatic assumption has been used to eliminate derivatives of ρ_1 . It is not assumed that the background quantities or their variations are small. Letting the four-component vector $u^{[i]}$ denote the field variables with $u^{[i]} \equiv v_i$ for $i = 2, 3, 4$, and $u^{[1]} \equiv p_1$, Eqs. (B.8a) and (B.8b) may be written in matrix form

$$L_{(1)}[u] + M \cdot u = 0, \quad (\text{B.9})$$

where $L_{(1)}[\dots]$ is a first-order differential operator acting on u while M is an ordinary matrix acting on u . In both cases these matrices depend on the background fields and the acoustic fields:

$$L_{(1)} = \begin{bmatrix} D^* & \rho_0 c^2 (\bar{\nabla})^T \\ \bar{\nabla} & 1_{3 \times 3} \rho_0 D^* \end{bmatrix}, \quad M = \begin{bmatrix} c^{-2} \bar{\nabla} \cdot \bar{w} + D^* c^{-2} & (\bar{\nabla} \rho_0)^T \\ c^{-2} D^* \bar{w} & \rho_0 \bar{\nabla} \otimes \bar{w} \end{bmatrix}.$$

One can see by inspection that the first terms in Eqs. (B.8a) and (B.8b) resemble Eqs. (B.1a) and (B.1b), leading to the conclusion that the characteristic condition for acoustic perturbations in the presence of background fluid motion is given by Eq. (B.5a), where the terms in the metric contain the background \bar{w} instead of \bar{v} .

B.3 The Eikonal Approximation, Acoustic Rays

Applying D to Eq. (B.1a) after dividing through by ρc^2 , taking the divergence of Eq. (B.1b), and taking the difference of the resulting equations, leads to

$$D \frac{1}{\rho c^2} D p - \bar{\nabla} \cdot \frac{1}{\rho} \bar{\nabla} p + \Delta_1 = 0, \quad (\text{B.10a})$$

while taking the gradient of Eq. (B.1a) and applying D to Eq. (B.1b) leads to

$$D \rho D \bar{v} - \bar{\nabla} \rho c^2 \bar{\nabla} \cdot \bar{v} + \bar{\Delta}_2 = 0, \quad (\text{B.10b})$$

where $\Delta_1 \equiv -\partial_k v_j \partial_j v_k$ and $\bar{\Delta}_2 \equiv -\partial_k p \bar{\nabla} v_k$. Applying the same procedure to Eqs. (B.8a) and (B.8b) leads to a similar result for the linear acoustic field in the presence of background motion:

$$\left\{ D^* \frac{1}{\rho_0 c^2} D^* p_1 - \bar{\nabla} \cdot \frac{1}{\rho_0} \bar{\nabla} p_1 \right\} + \tilde{\Delta}_1 = 0, \quad (\text{B.11a})$$

$$\left\{ D^* \rho_0 D^* \bar{v} - \bar{\nabla} \rho_0 c^2 \bar{\nabla} \cdot \bar{v} \right\} + \tilde{\Delta}_2 = 0, \quad (\text{B.11b})$$

where

$$\begin{aligned} \tilde{\Delta}_1 \equiv & D^* \left(\frac{p_1}{\rho_0 c^2} \bar{\nabla} \cdot \bar{w} \right) - \bar{\nabla} \cdot \left(\frac{p_1}{\rho_0 c^2} D^* \bar{w} \right) + D^* (\bar{v} \cdot \bar{\nabla} \ln \rho_0) + D^* \left(\frac{p_1}{\rho_0} D^* c^{-2} \right) \\ & - \partial_k (\bar{v} \cdot \bar{\nabla} w_k) - \partial_k v_j \partial_j w_k, \end{aligned}$$

$$\tilde{\Delta}_2 \equiv D^* (\rho_0 \bar{v} \cdot \bar{\nabla} \bar{w}) + D^* (\rho_1 D^* \bar{w}) - \bar{\nabla} (p_1 \bar{\nabla} \cdot \bar{w}) - \bar{\nabla} (c^2 \bar{v} \cdot \bar{\nabla} \rho_0) - \partial_k p_1 \bar{\nabla} w_k.$$

The equation for the eikonal in the high-frequency limit of linear acoustics, like that for the bicharacteristics, comes from the highest-order derivatives. The terms $\tilde{\Delta}_1$ and $\tilde{\Delta}_2$ contain only the field variables and first-order derivatives. The eikonal approximation is defined by taking $\alpha \rightarrow 0$, $p_1 = \pi_\alpha e^{i\varphi/\alpha}$ and $\bar{v} = \bar{\sigma}_\alpha e^{i\varphi/\alpha}$, with $\pi_\alpha \equiv \pi_0 + \alpha \pi_1 + \dots$, $\bar{\sigma}_\alpha \equiv \bar{\sigma}_0 + \alpha \bar{\sigma}_1 + \dots$, where complex fields have been used for simplicity. Inserting these

expansions for the field variables and collecting all terms of order α^{-2} leads to the following eikonal equation in matrix form:

$$\begin{bmatrix} -H_2 & 0^T \\ 0 & B \end{bmatrix} \begin{pmatrix} \pi_0 \\ \bar{\sigma}_0 \end{pmatrix} = 0, \quad (\text{B.12})$$

where H_2 is defined in Eq. (B.3) and $B \equiv c^2 \bar{\nabla} \varphi \otimes \nabla \varphi - 1_{3 \times 3} (D^* \varphi)^2$. Defining $Q \equiv -H_2 \oplus B$ for the block-diagonal matrix in Eq. (B.12), the condition for the existence of a nontrivial solution to Eq. (B.12), $\det Q = -H_2 \det B = 0$, leads to the condition

$$Q = (D^* \varphi)^4 \left((D^* \varphi)^2 - c^2 \bar{\nabla} \varphi \cdot \bar{\nabla} \varphi \right)^2 = 0. \quad (\text{B.13})$$

By inspection of the terms $\tilde{\Delta}_1$ and $\tilde{\Delta}_2$, one sees that they may be set to zero in the limit of a slowly varying environment since every term contains derivatives of the background fluid variables. This leads to a decoupling of the equations:

$$D^* \frac{1}{\rho_0 c^2} D^* p_1 - \bar{\nabla} \cdot \frac{1}{\rho_0} \bar{\nabla} p_1 \approx 0, \quad (\text{B.14a})$$

$$D^* \rho_0 D^* \bar{v} - \bar{\nabla} \rho_0 c^2 \bar{\nabla} \cdot \bar{v} \approx 0. \quad (\text{B.14b})$$

B.4 Time-Parameterized Rays in Three Dimensions

The surface of constant time $\varphi(\bar{x}, t)_{t=t_0} \equiv \varphi(\bar{x})$, generated by taking a constant time cross-section of the wavefront, is referred to as a phase surface (Fig. B1). (From here on, a wavefront is a surface of equal time, and ‘‘in phase’’ is taken to mean equal time of flight.)

In general, displacements in the null hypersurface are subject to the constraint $g_{00} dt^2 + g_{ij} dx^i dx^j + 2g_{0i} dt dx^i = 0$, which leads to the following constraint on $d\bar{x}/dt$:

$$\frac{g_{ij}}{g_{00}} \frac{dx^i}{dt} \frac{dx^j}{dt} + 2 \frac{g_{0i}}{g_{00}} \frac{dx^i}{dt} = -1. \quad (\text{B.15})$$

For the specific metric given in Eq. (B.5a), Eq. (B.15) states that the ray velocity relative to the moving fluid equals the local sound speed $(d\bar{x}/dt - \bar{v}) \cdot (d\bar{x}/dt - \bar{v}) = c^2$ (see Fig. B2).

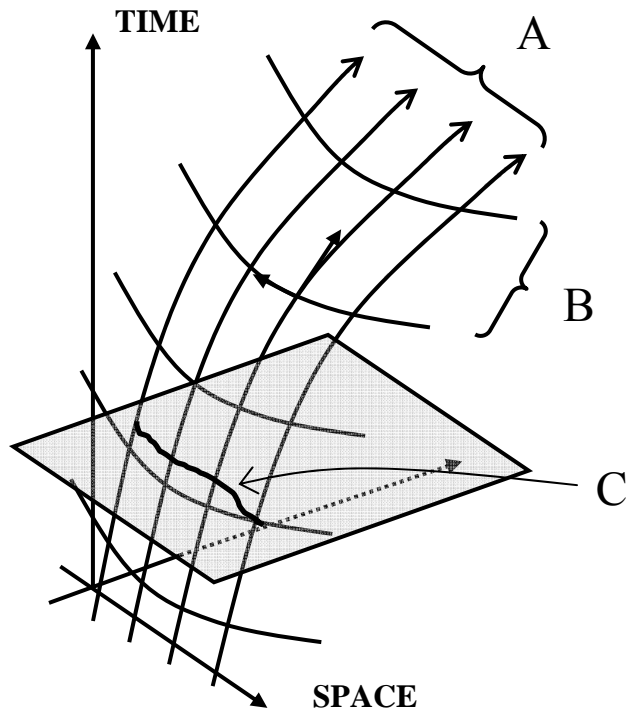


Figure B1. Sample of a complete space-time ray structure. (A) Family of geodesics labeled by s , where the s parameterized flow lines are constructed from the deviation vector acting on a fiducial geodesic. (B) Each flow line represents a curve of constant affine parameter. A tangent vector and the deviation at a single point are illustrated. (C) A curve of equal-time (wavefront) constructed from the intersection of a constant time plane with the geodesic flow. Equal-parameter curves do not lie in the constant time surface in general.

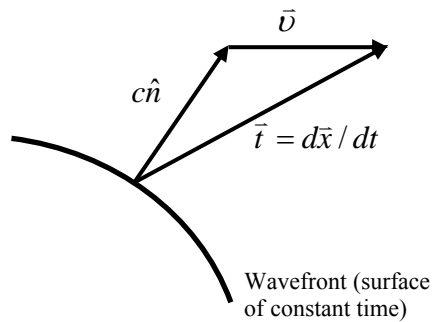


Figure B2. Relationship between the fluid velocity, ray tangent, and wavefront normal in Euclidean space.

An equation for $d\bar{x}/dt$ is derived from Eq. (B.7) by writing the equations for time and space separately:

$$\frac{d^2 x^k}{d\lambda^2} + \Gamma^k_{ij} \frac{dx^i}{d\lambda} \frac{dx^j}{d\lambda} + \Gamma^k_{00} \frac{dt}{d\lambda} \frac{dt}{d\lambda} + 2\Gamma^k_{i0} \frac{dx^i}{d\lambda} \frac{dt}{d\lambda} = 0, \quad (\text{B.16a})$$

$$\frac{d^2 t}{d\lambda^2} + \Gamma^0_{ij} \frac{dx^i}{d\lambda} \frac{dx^j}{d\lambda} + \Gamma^0_{00} \frac{dt}{d\lambda} \frac{dt}{d\lambda} + 2\Gamma^0_{i0} \frac{dx^i}{d\lambda} \frac{dt}{d\lambda} = 0. \quad (\text{B.16b})$$

Changing the parameter along the ray from λ to t leads to

$$\frac{d^2 x^k}{dt^2} + \frac{d^2 t/d\lambda^2}{(dt/d\lambda)^2} \frac{dx^k}{dt} + \Gamma^k_{ij} \frac{dx^i}{dt} \frac{dx^j}{dt} + \Gamma^k_{00} + 2\Gamma^k_{i0} \frac{dx^i}{dt} = 0, \quad (\text{B.17a})$$

$$\frac{d^2 t/d\lambda^2}{(dt/d\lambda)^2} + \Gamma^0_{ij} \frac{dx^i}{dt} \frac{dx^j}{dt} + \Gamma^0_{00} + 2\Gamma^0_{i0} \frac{dx^i}{dt} = 0. \quad (\text{B.17b})$$

Using Eq. (B.17b) to replace the second term in Eq. (B.17a) gives

$$\begin{aligned} \frac{d^2 x^k}{dt^2} - \left(\Gamma^0_{ij} \frac{dx^i}{dt} \frac{dx^j}{dt} + \Gamma^0_{00} + 2\Gamma^0_{i0} \frac{dx^i}{dt} \right) \frac{dx^k}{dt} \\ + \Gamma^k_{ij} \frac{dx^i}{dt} \frac{dx^j}{dt} + \Gamma^k_{00} + 2\Gamma^k_{i0} \frac{dx^i}{dt} = 0. \end{aligned} \quad (\text{B.18})$$

Using the Christoffel symbols, Appendix D, and some algebra, the equation for the 3-dimensional ray paths as a function of time becomes

$$\begin{aligned} \ddot{x}_k = \frac{(\dot{x}_k - v_k)}{2c^2} S_{ij} (\dot{x}_i - v_i) (\dot{x}_j - v_j) + (\dot{x}_k - v_k) (d_{-\bar{v}} \ln c + 2\dot{\bar{r}} \cdot \bar{\nabla} \ln c) \\ + \partial_t v_k - c \partial_k c - \omega_{kj} (\dot{x}_j - v_j) + \frac{1}{2} (S_{kj} - \omega_{kj}) v_j. \end{aligned} \quad (\text{B.19})$$

Equation (B.19) is converted to an equation for the wavefront normal through the identification $c\hat{n} \equiv \dot{\bar{x}} - \bar{v}$, and can be used to determine either the evolution of $\dot{\bar{x}}$ or \hat{n} :

$$\frac{d}{dt} \hat{n}_k + \Omega_{ki} \hat{n}_i = 0, \quad (\text{B.20})$$

where $\Omega_{ki} \equiv \frac{1}{2} \varepsilon_{jki} (\bar{\nabla} \times \bar{v} + \bar{s} \times \hat{n} + 2\bar{\nabla} c \times \hat{n})_j$.

Along with a complete presentation of the bicharacteristics and a discussion of the variety of situations described by null geodesics, the main results of this appendix are Eqs. (B.7), (B.19), and (B.20). In particular, note that the geodesics determined by Eq. (B.7) describe the propagation of discontinuities and the evolution of the wavefront in the most general situations, for nonlinear disturbances propagating in a random environment. The catch-22 is that in order to find these curves in the nonlinear case one needs the complete velocity field, $\vec{v} = \vec{v} + \vec{w}$, which requires knowing the complete solution in the first place.

Appendix C

CONSTRUCTION OF THE INTERNAL FRAME FIELD

C.1 Ray-Centered Frame in Space-Time

To calculate the geometric spreading of an acoustic beam from the deviation equation the Riemann tensor must be projected into a ray-centered frame field. The frame being defined formally on the null hypersurface requires a basis of four mutually orthogonal vectors in space-time. Following the notation in Hawking *et al.*³², the ray tangent, T^μ , is chosen to serve as one of the coordinate directions. A second null vector, L^μ , satisfying the condition $L^\mu T^\nu g_{\mu\nu} = -1$, is chosen as the second basis vector. To complete the local geodesic coordinate basis, two space-like directions, e_1^α and e_2^β , satisfying the conditions $T^\alpha e_{1\alpha} = 0$, $L^\alpha e_{1\alpha} = 0$, and $e_I^\alpha e_{J\alpha} = \delta_{IJ}$ for $I, J = 1, 2$, are introduced.

The two null vectors define a time-like direction $E_t = c^{-1}(1 \ \bar{v})$ that is orthogonal to the two-dimensional space-like hypersurface $\langle \hat{e}_I \rangle$ at all points in space-time. After defining this pseudo-orthonormal basis at an initial point on $\gamma_F(\lambda)$, the basis is parallel transported along $\gamma_F(\lambda)$ to define a new basis at each point by solving the parallel transport equation:

$$\frac{d(\hat{e}_I)^\alpha}{d\lambda} + \Gamma^\alpha_{\ \mu\nu} T^\mu (\hat{e}_I)^\nu = 0. \quad (\text{C.1})$$

The null vector L^μ is automatically parallel transported along the null geodesic T^μ .

To ensure that neighboring rays are emitted from the source at the same “time” as the fiduciary ray, the initial space-like basis is chosen to be purely spatial in the coordinate frame, $(\hat{e}_I)^\mu = (0 \ \hat{e}_I)$, and the initial deviation $Y_0^\mu = (0 \ \bar{Y}_0)$ is chosen to lie along one of the initial basis vectors.

Equation (C.1) formally preserves the constraints placed on the initial conditions. Beginning with 16 quantities, 4 vectors with 4 components each, the conditions impose 11 constraints leaving 5 independent quantities. Four of these are the components of T^μ determined by the geodesic equation, leaving only one remaining quantity to calculate. The vector L^μ may be determined algebraically in terms of the environmental parameters. The remaining degree of freedom may be identified with a two-dimensional rotation of the space-like basis $\{\hat{e}_I\}$ in the $\langle \hat{e}_I \rangle$ hyperplane expressed as $R_{IJ}^\theta e_{J0}$.

C.2 Ray-Centered Frame in Cartesian Space, Wavefront Normal Basis

In this section an alternate choice of internal basis is presented. This representation, termed auxiliary basis, is better suited for visualization and interpretation of the deviation, as it always remains tangent to the surface of constant phase in space. From the conditions $T^\mu \hat{e}_I^\nu g_{\mu\nu} = 0$ and $\hat{e}_I^\mu \hat{e}_I^\nu g_{\mu\nu} = 1$, one may verify that

$$\hat{n} \cdot (\hat{e}_I - \hat{e}_I^0 \bar{t}) = 0, \quad \|\hat{e}_I - \bar{t} \hat{e}_I^0\| = 1, \quad (\text{C.2})$$

with respect to the ordinary dot product in three-dimensional space. Hence the set of three-dimensional vectors

$$\tilde{e}_I^k \equiv \hat{e}_I^k - \hat{e}_I^0 \frac{dx^k}{dt} \quad (\text{C.3})$$

is tangent to the wavefront everywhere along the ray and the basis (\hat{n}, \tilde{e}_I) remains orthonormal as it is propagated along the ray. The vectors \tilde{e}_I are referred to here as an auxiliary basis. An equal-time deviation is constructed by projecting the components Y_I onto the auxiliary basis. The deviation projected into the different basis will point in different directions in four dimensions but the magnitude is independent of the choice of basis, $\|\tilde{Y}\| = \sqrt{Y^\mu Y_\mu} = \sqrt{Y_1^2 + Y_2^2}$.

The sectional curvature needed for the spreading equation may be rewritten as $4K_{IJ} = R_{\mu\nu\alpha\beta} \Lambda_I^{\mu\nu} \Lambda_J^{\alpha\beta}$, where $\Lambda_I^{\mu\nu} \equiv T^\mu \hat{e}_I^\nu - T^\nu \hat{e}_I^\mu$. The mixed components of this tensor,

$$\Lambda_I^{0k} = T^0 \hat{e}_I^k - T^k \hat{e}_I^0 = T^0 (\hat{e}_I^k - \hat{e}_I^0 (dx^k/dt)) = T^0 \tilde{e}_I^k, \quad (\text{C.4a})$$

are clearly proportional to the auxiliary basis. The pure space components,

$$\Lambda_I^{ik} = T^i \hat{e}_I^k - T^k \hat{e}_I^i = T^i \tilde{e}_I^k - T^k \tilde{e}_I^i, \quad (\text{C.4b})$$

are equal to the components of the cross product $\bar{T} \times \tilde{e}_I$ in three dimensions. The tensor $\Lambda_I^{\mu\nu}$ is parallel transported along $\gamma(\lambda)$,

$$\frac{d}{d\lambda} \Lambda_I^{\mu\nu} + \Gamma^\mu_{\alpha\beta} T^\alpha \Lambda_I^{\beta\nu} + \Gamma^\nu_{\alpha\beta} T^\alpha \Lambda_I^{\mu\beta} = 0. \quad (\text{C.5})$$

Equation (C.5) tracks six fields, counting indices in four dimensions. It is clear from the definition of $\Lambda_I^{\mu\nu}$ that there are only three degrees of freedom. By separating Eq. (C.5)

into individual components, the following transport equation for the auxiliary basis \tilde{e}_l^k in E^3 is derived:

$$\frac{d}{dt}\tilde{e}_l^k + \frac{1}{2}\varepsilon_{jki}(\bar{\nabla} \times \bar{v} + \bar{s} \times \hat{n} + 2\bar{\nabla}c \times \hat{n})_j \tilde{e}_l^i = 0, \quad (\text{C.6})$$

with $s_k \equiv n_j S_{jk}$. Note that an overall factor of $dt/d\lambda$ has been divided out. In principle, the parallel transport equation has a solution in terms of a path-ordered integral involving the SO(3) generator evaluated along the ray. In practice, these are not known in closed form. However, assuming that the ray equation has been solved either analytically or numerically the normal \hat{n} is known, reducing the problem to a two-dimensional rotation about the wavefront normal followed by an application two Euler matrices to orient the basis along the ray path.

Choosing the initial basis to match a global Cartesian-coordinate basis $\langle \hat{n}(0) \tilde{e}_1(0) \tilde{e}_2(0) \rangle = \langle i \ j \ k \rangle$, the rotation matrix taking $\hat{n}(0) \rightarrow \hat{n}$ may be found explicitly. The rotation of $\langle \tilde{e}_l \rangle$ about \hat{n} is denoted $R(\alpha)$. The action of this sequence on the initial basis vectors, interpreted as an active transformation on the initial values $\langle \hat{n}(0) \tilde{e}_l(0) \rangle$, is denoted $U = R(\varphi)R(\theta)R(\alpha)$. The rotation $R(\alpha)$ has a block-diagonal form $R(\alpha) = 1 \oplus r$, where r is a two-dimensional rotation about the x -axis of the global coordinate system. Inserting this into Eq. (C.6) leads to the following differential equation for r :

$$\frac{dr}{dt} + \tilde{\omega}\sigma_x r = 0, \quad (\text{C.7})$$

where $\sigma_x = \begin{pmatrix} 0 & -1 \\ 1 & 0 \end{pmatrix}$, $\tilde{\omega} \equiv \frac{n_y \Omega_{xz} - n_x \Omega_{yz}}{n_x^2 + n_y^2}$.

The solution to Eq. (C.7) is

$$r = \begin{pmatrix} \cos \alpha & -\sin \alpha \\ \sin \alpha & \cos \alpha \end{pmatrix}, \quad (\text{C.8})$$

where $\alpha = \int \tilde{\omega}|_y dt$, with the integrand evaluated along the specific ray path in space. The dependence of $\tilde{\omega}$ on specific Cartesian indices comes from the choice of lining up the initial basis with the global coordinate system.

Equation (C.8) reduces the problem of tracking eight degrees of freedom plus constraints to one of evaluating a single integral. This reduction is not without cost. It is clear that the denominator will vanish whenever a ray has a horizontal turning point. While this may not happen often in modeling underwater systems where attention is

focused on parabolic rays trapped in sound ducts, it will happen in more general situations. The danger of this divergence occurring indicates that it may be more practical to track the components of the larger dynamical system, using the constraints to regulate error along the way.

The ability to reduce Eq. (C.1) to Eq. (C.7) depends on the identification of $\Lambda_I^{\mu\nu}$ with the wavefront normal basis. In general, this trick may always be employed to reduce the number of quantities needed to calculate the sectional curvature and is invaluable in 2-dimensional ray systems, 3-dimensional space-time systems, as it allows one to generate \tilde{e} by rotating \hat{n} by 90° . Without this insight one would be compelled to either track all three components of e by Eq. (C.1) or evaluate Eq. (C.8).

Appendix D

RIEMANN TENSOR AND CHRISTOFFEL SYMBOLS FOR THE ACOUSTIC METRIC

For the acoustic metric defined by the characteristic condition, Eq. (B.5),

$$g^{\mu\nu} \equiv \frac{1}{c^2} \begin{pmatrix} -1 & -v_i \\ -v_j & c^2 \delta_{ji} - v_j v_i \end{pmatrix}, \quad g_{\mu\nu} = \begin{pmatrix} -c^2 + v^2 & -v_i \\ -v_j & \delta_{ji} \end{pmatrix},$$

direct substitution into Eqs. (A.4) and (A.10) lead to the following:

$$\Gamma^0_{00} = d_{-\bar{v}} \ln c + \frac{v_i v_j}{2c^2} S_{ij}, \quad (D.1a)$$

$$\Gamma^0_{i0} = \partial_i \ln c - \frac{v_j}{2c^2} S_{ij}, \quad (D.1b)$$

$$\Gamma^i_{00} = v_i d_{-\bar{v}} \ln c - \partial_i v_i + c \partial_i c - \frac{1}{2} v_j \omega_{ij} - \frac{v_j}{2c^2} (c^2 \delta_{ki} - v_k v_i) S_{jk}, \quad (D.1c)$$

$$\Gamma^i_{j0} = v_i \partial_j \ln c + \frac{1}{2} \omega_{ij} - \frac{v_i v_k}{2c^2} S_{jk}, \quad (D.1d)$$

$$\Gamma^k_{ij} = v_k \Gamma^0_{ij} = \frac{v_k}{2c^2} S_{ij}, \quad (D.1e)$$

and

$$R_{nimj} = \frac{1}{4c^2} (S_{mn} S_{ij} - S_{mi} S_{nj}), \quad (D.2a)$$

$$R_{0ikj} = \frac{1}{2} (\partial_j S_{ik} - \partial_k S_{ij}) + \frac{1}{2} (S_{ij} \partial_k \ln c - S_{ik} \partial_j \ln c) + \frac{v_n}{4c^2} (S_{ik} S_{jn} - S_{ij} S_{kn}), \quad (D.2b)$$

$$\begin{aligned} R_{0i0j} = & -\frac{1}{2} \partial_t S_{ij} - \frac{1}{2} v_n (\partial_j S_{in} + \partial_j \omega_{in}) + c \partial_i \partial_j c + \frac{1}{2} S_{ij} \partial_t \ln c - \frac{v_n v_m}{4c^2} S_{in} S_{jm} \\ & + \frac{v_n}{2} (S_{jn} \partial_i \ln c + S_{in} \partial_j \ln c - S_{ij} \partial_n \ln c) - \frac{1}{4} (S_{im} S_{jm} + \omega_{im} S_{jm} + \omega_{jm} S_{im}). \end{aligned} \quad (D.2c)$$

Typically the Riemann tensor contains second derivatives of the metric components as well as first derivatives squared. A significant feature of this system is the lack of second-order time derivatives of the environmental parameters and the coupling of $\partial_t c$ to the fluid velocity. For a stationary medium the focusing is determined solely by the spatial derivatives of the sound speed.

Appendix E

FERMAT'S PRINCIPLE AND SNELL'S LAW

E.1 Fermat's Principle

Fermat's principle follows immediately from the line element by solving for dt :

$$dt = \frac{\sqrt{(\bar{v} \cdot d\bar{r})^2 + (c^2 - v^2)d\bar{r} \cdot d\bar{r}} - \bar{v} \cdot d\bar{r}}{c^2 - v^2}, \quad (\text{E.1})$$

where the + root is taken for subsonic flow. For supersonic flow, $d\bar{r} \cdot \bar{v} > 0$ and the travel times are determined by the – root.

E.2 Metric Symmetry and Snell's Law

An isometry (symmetry of the metric) is indicated by a cyclic coordinate³⁰. The presence of a cyclic coordinate in the metric, labeled x^C , leads to a conservation law for the corresponding momentum or conjugate variable,

$$\frac{dp_C}{d\lambda} = \frac{dg_{C\beta}T^\beta}{d\lambda} = \frac{d\xi_C^\alpha g_{\alpha\beta}T^\beta}{d\lambda} = 0. \quad (\text{E.2})$$

The vector ξ_C^α , called a Killing vector, points in the direction of the x^C coordinate curves. (The statement "...presence of a cyclic coordinate" x^C is equivalent to the absence of that coordinate from the metric altogether.) When there is enough symmetry, the second-order geodesic equations are reducible to a set of first-order equations.

Specializing to a time-independent environment, the Killing vector $\xi_t^\alpha = (1 \ \bar{0})$ leads to the conservation law

$$-(c^2 - v^2)\frac{dt}{d\lambda} - \bar{v} \cdot \frac{d\bar{r}}{d\lambda} = \kappa_0. \quad (\text{E.3})$$

Traditionally, this is associated with the energy of the particle, and for the metric signature in Eq. (B.5) κ_0 is negative. (From here on, $\kappa_0 > 0$ and an overall minus sign is dropped from Eq. (E.3).) Consider the problem of a layered medium where c and \bar{v} depend on only one Cartesian coordinate, z . There are two more conserved currents,

which may be thought of as components of the ray's translational momentum. The Killing vectors \hat{i} and \hat{j} lead to

$$\frac{d\bar{r}}{d\lambda} - \frac{dt}{d\lambda} \bar{v}_T = \bar{\kappa}, \quad (\text{E.4})$$

where $\bar{\kappa} \equiv \kappa_1 \hat{i} + \kappa_2 \hat{j}$ and $\bar{v}_T \equiv v_x \hat{i} + v_y \hat{j}$. Imposing the null constraint on the components of the tangent vector leads to

$$-c^2 \dot{t}^2 + \bar{\kappa} \cdot \bar{\kappa} + (\dot{z} - v_z \dot{t})^2 = 0 \quad (\text{E.5})$$

and

$$c^2 \dot{t} = \kappa_0 - \bar{v}_T \cdot \bar{\kappa} - v_z (\dot{z} - v_z \dot{t}). \quad (\text{E.6})$$

Equations (E.3) and (E.4) may be used to derive a generalized version of Snell's law originally presented by Kornhauser¹⁴ for the special case $\bar{v}_T = v \hat{i}$. By definition Eq. (E.3) states that $\bar{\kappa} = ic \hat{n}_T$ which in turn states that the projection of the wavefront normal in the x - y plane points in a fixed direction. Equation (E.3) may be rewritten to give $\kappa_0 = \bar{T} \cdot c \hat{n} = ic(c + \bar{v} \cdot \hat{n})$, relating the energy to the angle between the wavefront normal and the spatial component of the ray. When $\bar{v} = \bar{v}_T = v \hat{i}$, Eq. (E.6) becomes $\kappa_0 = ic(c + v n_x)$. Taking the momentum-to-energy ratio in this case gives Snell's law for the wavefront normal:

$$\frac{\cos \theta}{c + v \cos \theta} = \alpha, \quad (\text{E.7})$$

with $\alpha \equiv \kappa_1 / \kappa_0$ and $n_x \equiv \cos \theta$. The ray angle is related to θ by $c \cos \theta + v = \dot{r} \cos \psi$. The magnitude of the ray velocity follows from the null constraint

$$\dot{r} = v \cos \psi + \sqrt{c^2 - v^2 \cos^2 \psi}. \quad (\text{E.8})$$

Insertion of Eq. (E.8) into Eq. (E.7) gives Kornhauser's result for Snell's law:

$$\alpha = \frac{1 - \varepsilon \sin^2 \psi + \cos \psi \sqrt{1 - \varepsilon^2 \sin^2 \psi}}{c \left(1 - \varepsilon^2 \sin^2 \psi + \cos \psi \sqrt{1 - \varepsilon^2 \sin^2 \psi} \right)}. \quad (\text{E.9})$$

The paths of the rays propagating in a layered media with $v_z = 0$ are

$$\frac{dt}{d\lambda} = \frac{(\kappa_0 - \bar{v}_T \cdot \bar{\kappa})}{c^2}, \quad (\text{E.10})$$

$$\frac{d\bar{r}}{d\lambda} = \bar{\kappa} + \frac{v}{c^2}(\kappa_0 - \bar{v}_T \cdot \bar{\kappa}), \quad (\text{E.11})$$

$$\frac{dz}{d\lambda} = \pm \frac{\sqrt{(\kappa_0 - \bar{v}_T \cdot \bar{\kappa})^2 - \bar{\kappa} \cdot \bar{\kappa} c^2}}{c}. \quad (\text{E.12})$$

Taking appropriate ratios of Eqs. (E.10) and (E.11) leads immediately to the ray-path integrals encountered in underwater acoustics.

The procedure may be generalized to any set of coordinates. A derivation of two-dimensional Snell's law in polar coordinates is now presented. The acoustic line element in polar coordinates is

$$-(c^2 - v^2)dt^2 - 2v_r dr dt - 2v_\theta r d\theta dt + dr^2 + r^2 d\theta^2 = 0. \quad (\text{E.13})$$

Specializing to a rotationally symmetric, time-independent environment with $\bar{v} = v\hat{\theta}$, leads to the following set of equations for the ray:

$$c^2 r^2 \dot{r}^2 = -\alpha^2 + (r - \alpha v)^2, \quad (\text{E.14})$$

$$c^2 r^2 \dot{\theta} = \alpha c^2 + v(r - \alpha v), \quad (\text{E.15})$$

$$c^2 r \dot{t} = (r - \alpha v). \quad (\text{E.16})$$

Following all the same steps leads to the same result for Snell's law, Eq. (E.9), with θ interpreted as the instantaneous angle between the wavefront normal and $\hat{\theta}$.